C Journal of Carbon Research

MDPI

Article

Applicability and Limitations of Ru's Formulation for Vibration Modelling of Double-Walled Carbon Nanotubes

Matteo Strozzi

Department of Sciences and Methods for Engineering, University of Modena and Reggio Emilia, Via Giovanni Amendola 2, 42122 Reggio Emilia, Italy; matteo.strozzi@unimore.it

Abstract: In this paper, a comparison is conducted between two different formulations of the van der Waals interaction coefficient between layers, as applied to the vibrations of double-walled carbon nanotubes (DWCNTs); specifically, the evaluation of the natural frequencies is achieved through Ru's and He's formulations. The actual discrete DWCNT is modelled by means of a couple of concentric equivalent continuous thin cylindrical shells, where Donnell shell theory is adopted to obtain strain-displacement relationships. In order to take into account the chirality effect of DWCNT, an anisotropic elastic shell model is considered. Simply supported boundary conditions are imposed and the Rayleigh–Ritz method is used to obtain approximate natural frequencies and mode shapes. A parametric analysis considering different values of diameters and numbers of waves along longitudinal and circumferential directions is performed by adopting Ru's and He's formulations. From the comparisons, it is evident that Ru's formulation provides unsatisfactory results for relatively low values of diameters and relatively high numbers of circumferential waves with respect to the more accurate He's formulation. This behaviour is observed for every number of longitudinal half-waves. Therefore, Ru's formulation cannot be used for the vibration modelling of DWCNTs in a large range of diameters and wavenumbers.

Keywords: carbon nanotubes; vibration modelling; Donnell shell theory; anisotropic elastic shell model; van der Waals interaction forces; Ru's formulation

Citation: Strozzi, M. Applicability and Limitations of Ru's Formulation for Vibration Modelling of Double-Walled Carbon Nanotubes. *C* **2022**, *8*, 59. https://doi.org/10.3390/c8040059

Academic Editor: Jandro L. Abot

Received: 13 September 2022
Accepted: 31 October 2022
Published: 2 November 2022

1. Introduction

Carbon nanotubes (CNTs) were discovered in 1991 inside the NEC Corporation laboratories by S. Iijima, who studied the synthesis of fullerenes and first prepared a new type of carbon structures, referred to as CNTs, which were described as "helical microtubules of graphitic carbon" [1]. Since CNTs have very high Young's modulus and tensile strength, together with very small diameter, then they can reach the natural frequencies of the THz order and therefore can be used as ultra-high sensitivity resonators in many electro-mechanical devices, such as sensors, charge detectors and oscillators [2]. In addition, the extremely high electrical and thermal conductivity of CNTs, together with the very high transparency in a visible range, makes them promising candidates for innovative applications including heat exchangers and energy conversion systems, with the role of advanced catalyst supports or electrodes in solar and fuel cells [3,4].

Due to their relevant applications in several mechanical components, vibrations of CNTs have attracted much attention from Researchers. Specifically, CNT vibrations have been studied by means of experiments, atomistic mechanic simulations and continuum mechanic models. Resonant Raman spectroscopy (RRS) starts from the experimental measurement of CNT diameter by means of atomic force microscopy and investigates the atomic structure, chirality and natural frequencies of CNTs [5–7]. However, due to high technological complexity and costs, experimental methods cannot be considered efficient approaches to studying the mechanical behaviour of CNTs. Molecular

dynamics (MD) simulations consider CNT atoms as interacting point-like masses, where the vibrations of the free atoms are recorded for a certain time duration at a fixed temperature [8–10]. However, due to the high computational effort, atomistic mechanics methods cannot be easily applied to the structural simulation of CNTs, which incorporate a large number of carbon atoms. Since theoretical models based on continuum mechanics are computationally more efficient than MD simulations and do not present the technological complexity and high costs of RRS, then continuous elastic models are the most commonly adopted methods for the study of CNT vibrations. In these models, it is assumed that the effective discrete structure of CNTs can be replaced by an equivalent homogeneous elastic structure with a continuous distribution of mass and stiffness, not considering their intrinsic atomic nature and so reducing the number of degrees of freedom [11–13].

In order to carefully investigate the validity of continuum mechanic approaches for the study of CNT vibrations, in the cases when the actual discrete CNT is modelled via an equivalent continuous thin cylindrical shell, some relevant open issues should be taken into account and properly discussed.

The first relevant issue to be taken into account in the modelling of CNTs as continuous elastic shells is given by anisotropy. CNTs are usually modelled as isotropic elastic shells [14–21]; however, they have a chirality-induced anisotropic behaviour due to their discrete nature that cannot be properly captured by using an isotropic shell model. To this aim, Chang et al. [22,23] developed a molecular mechanics model, called "stick-spiral model", able to correctly predict the chirality and size-dependent elastic properties of CNTs. They found explicit expressions for longitudinal Young's modulus and Poisson's ratio, circumferential Young's modulus and Poisson's ratio, and longitudinal shear modulus in the case of chiral CNTs. This molecular-based anisotropic elastic shell model including chirality effects was validated via comparisons with RRS and MD data, proving that the classical relationship of isotropic elastic continuum mechanics between Young's and shear modulus is not valid for CNTs. Ghavanloo and Fazelzadeh [24,25], starting from the results of [23], developed an anisotropic elastic shell model including chirality effects to study the vibration characteristics of CNTs. By applying the Flügge thin shell theory and complex method, they obtained the natural frequencies of radial breathing, torsional, longitudinal and radial modes under different CNT diameters and chiralities. Finally, they validated their model by means of comparisons with experimental RRS and numerical MD simulation data from the literature. In the present paper, the molecular mechanics-based anisotropic elastic shell model developed by Chang [22,23], and then refined by Ghavanloo and Fazelzadeh [24,25], for SWCNTs is extended to DWCNTs. Readers interested in deepening vibrations and stability of circular cylindrical shells can refer to the fundamental books of Leissa [26], Yamaki [27], Soedel [28] and Ventsel [29], where the strain-displacement relationships of the most important thin shell theories together with the related equations of motion and natural frequencies under different boundary conditions are reported. CNTs are divided into two main classes: single-walled carbon nanotubes (SWCNTs), given by graphene sheets rolled into cylinders, and multi-walled carbon nanotubes (MWCNTs), composed by concentric SWNTs, where the different cylinders are connected by van der Waals interaction forces.

In addition to anisotropy, in the specific case of MWCNTs, another relevant issue to be taken into consideration in the modelling of CNTs as continuous elastic shells is given by the simulation of van der Waals interaction forces between the concentric SWCNTs. The two most relevant formulations of van der Waals interaction forces in MWCNTs were developed by Ru and He. Both of them are based on the Lennard–Jones pair potential, which takes into account carbon–carbon potential depth, equilibrium separation distance and atom distance, where van der Waals interaction forces are obtained by deriving Lennard–Jones pair potential with respect to the carbon–carbon atom distance [30]. The pressure exerted on the ith SWCNT, as a function of the radial displacement, is obtained by integrating van der Waals interaction forces over the entire MWCNT.

Ru [31–33] proposed a linear relationship between pressure due to van der Waals interaction forces and radial displacement for the buckling and vibration analysis of MWCNTs in which the interaction coefficient is constant, i.e., it is not dependent on the radius of the individual SWCNT. In this model, the value of the interaction coefficient can be estimated using data given in [34], which are derived from the known van der Waals interaction between a carbon atom and a flat graphite sheet, and the van der Waals pressure between the inner and outer tube at any point is assumed to depend on the interlayer spacing at that point. By adopting Ru's formulation, Elishakoff and Pentaras [35,36] obtained fundamental natural frequencies of DWCNTs considering different boundary conditions and shell theories by adopting an isotropic elastic shell model. In particular, the results of Ref. [35], obtained by considering simply supported boundary conditions and Donnell shell theory, are adopted to validate the model proposed in the present paper in the isotropic case for Ru's formulation. Other relevant analytical studies on the linear vibrations of DWCNTs under different boundary conditions and geometries considering Ru's formulation are reported in Refs. [37–40]. However, it is clear that this simplified formulation is not accurate in modelling van der Waals interaction forces.

In order to accurately describe van der Waals interactions in MWCNTs, He [41–43] proposed a linear relationship between pressure due to van der Waals interaction forces and radial displacement where the interaction coefficient is radius dependent. By considering this refined formulation, natural frequencies of MWCNTs were analysed for different geometries and chiralities obtaining an excellent agreement with MD simulations. In particular, the results of Ref. [42], obtained by considering simply supported boundary conditions and the Donnell shell theory, are adopted to validate the model proposed in the present paper in the isotropic case for He's formulation. Strozzi and Pellicano [44–47] studied linear and nonlinear vibrations of MWCNTs considering He's formulation. The effect of geometry, boundary conditions and wavenumbers along longitudinal and circumferential directions on the natural frequencies were analysed. Applicability and limitations of the Donnell shell theory, with respect to the more accurate Sanders shell theory, were considered. The effect of nonlinear van der Waals interaction forces on the nonlinear response was investigated. Other interesting results on the linear vibrations of DWCNTs considering He's formulation are shown in Refs. [48–50], where the influence of boundary conditions and surrounding elastic medium on the resonant natural frequencies in case of noncoaxial vibration is studied. Moreover, in Refs. [51–55], some recent studies on vibrations and stability of DWCNTs, based on molecular dynamics simulations, non-local effect and anisotropic elastic model, are reported.

In the present paper, the comparison is conducted between Ru's and He's formulations of the van der Waals interaction coefficient for the evaluation of the natural frequencies of DWCNTs. The actual discrete DWCNT is modelled by means of a couple of concentric equivalent continuous cylindrical shells, where the Donnell shell theory is considered to obtain strain-displacement relationships. In order to take into account the chirality effects of DWCNTs, an anisotropic elastic shell model is used. Simply supported boundary conditions are imposed and the Rayleigh–Ritz method is adopted to obtain approximate natural frequencies and mode shapes. In the beginning, the results of the proposed model in the isotropic form are compared with data retrieved from the literature to check the validity of the shape functions used in the modal expansions of the displacement field. Then, the values of van der Waals interaction coefficient from Ru's and He's formulations are compared for different DWCNT diameters to verify the higher accuracy of He's formulation in simulating the actual anisotropic behaviour of DWCNTs. Starting from these results, considering an anisotropic elastic shell model and adopting Donnell shell theory, natural frequencies of DWCNTs with different diameters and wavenumber along longitudinal and circumferential directions obtained via Ru's and He's formulations are compared. Assuming the more accurate He's formulation as a reference, the applicability and limitations of Ru's formulation for the vibration modelling of DWCNTs are investigated.

2. Donnell Shell Theory for DWCNTs

In this paper, the actual discrete DWCNT shown in Figure 1a is modelled by means of a couple of concentric equivalent continuous cylindrical shells with van der Waals interactions between the layers. In Figure 1b,c, a single continuous cylindrical shell with radius R, length L and thickness h is shown; in order to describe the displacement field, a cylindrical coordinate system (O, x, θ, z) is adopted, due to the axisymmetric symmetry of the cylindrical shell, where the origin O of the reference system is located at the centre of one end of the shell. Three displacements are present: longitudinal $u(x, \theta, t)$, circumferential $v(x, \theta, t)$ and radial $w(x, \theta, t)$, where the radial displacement w is assumed to be positive outward; (x, θ) are the longitudinal and angular coordinates of an arbitrary point on the middle surface of the shell; z is the radial coordinate along the thickness h of the shell; t is the time variable. Starting from this continuum modelling, in the following, displacement field and strain-displacement relations for DWCNTs will be derived.

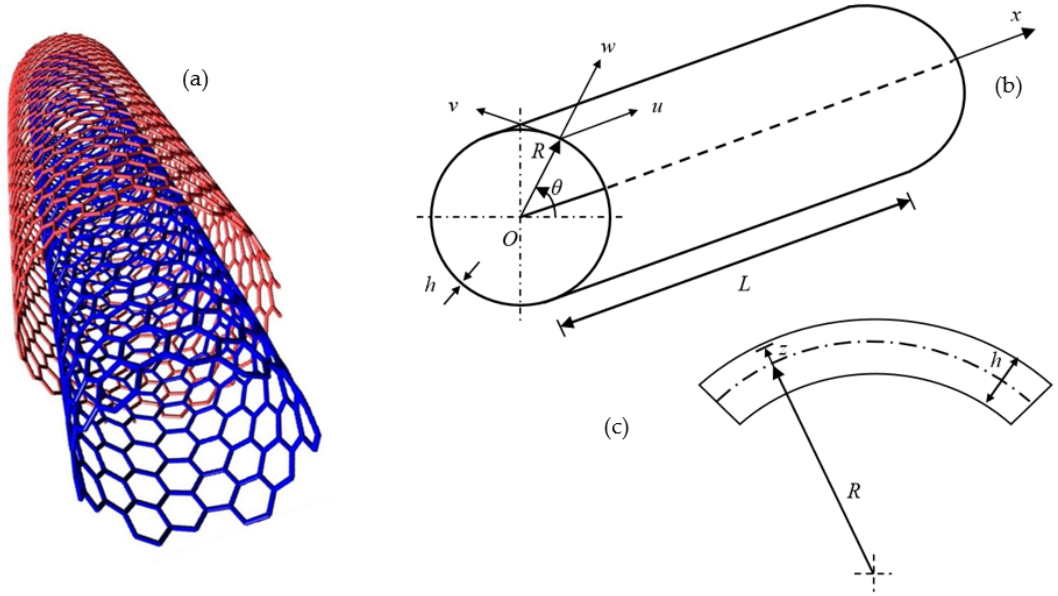

Figure 1. Continuum modelling of a DWCNT. (**a**) Actual discrete DWCNT; (**b**) geometry of the equivalent continuous thin circular cylindrical shell; (**c**) cross-section of the surface of the equivalent continuous shell.

2.1. Displacement Field

In order to avoid very fast time scales, which are due to the infinitesimal dimensions of CNTs, and therefore very hard convergence problems in the numerical integration, in this work, all dimensionless parameters are considered.

The dimensionless displacement field $(\tilde{u}_i, \tilde{v}_i, \tilde{w}_i)$ of the i-th cylindrical shell is written as [44]:

$$\tilde{u}_i = \frac{u_i}{R_i} \qquad \tilde{v}_i = \frac{v_i}{R_i} \qquad \tilde{w}_i = \frac{w_i}{R_i} \qquad i = 1,2 \qquad (1)$$

where (u_i, v_i, w_i) is the corresponding dimensional displacement field and R_i is the radius of the i-th shell.

2.2. Strain-Displacement Relationships

In this paper, the Donnell shell theory is adopted to obtain linear strain-displacement relationships.

The dimensionless middle surface strains of the i-th cylindrical shell $(\tilde{\varepsilon}_{x,0,i}, \tilde{\varepsilon}_{\theta,0,i}, \tilde{\gamma}_{x\theta,0,i})$ are written in the form [44]:

$$\tilde{\varepsilon}_{x,0,i} = \alpha_i \frac{\partial \tilde{u}_i}{\partial \eta} \qquad \tilde{\varepsilon}_{\theta,0,i} = \frac{\partial \tilde{v}_i}{\partial \theta} + \widetilde{w}_i \qquad \tilde{\gamma}_{x\theta,0,i} = \frac{\partial \tilde{u}_i}{\partial \theta} + \alpha_i \frac{\partial \tilde{v}_i}{\partial \eta} \qquad i = 1,2 \tag{2}$$

where $\eta = x/L$ is the dimensionless longitudinal coordinate of the shell and $\alpha_i = R_i/L$.

The dimensionless middle surface changes in curvature and torsion of the i-th cylindrical shell ($\tilde{k}_{x,i}, \tilde{k}_{\theta,i}, \tilde{k}_{x\theta,i}$) are written as [44]:

$$\tilde{k}_{x,i} = -\alpha_i^2 \frac{\partial^2 \widetilde{w}_i}{\partial \eta^2} \qquad \tilde{k}_{\theta,i} = -\frac{\partial^2 \widetilde{w}_i}{\partial \theta^2} \qquad \tilde{k}_{x\theta,i} = -2\alpha_i \frac{\partial^2 \widetilde{w}_i}{\partial \eta \partial \theta} \qquad i = 1,2 \tag{3}$$

The dimensionless strains in a generic point of the external surface of the i-th cylindrical shell ($\tilde{\varepsilon}_{x,i}, \tilde{\varepsilon}_{\theta,i}, \tilde{\gamma}_{x\theta,i}$) are related to the corresponding dimensionless middle surface strains and changes in curvature and torsion by means of the following relationships [44]:

$$\tilde{\varepsilon}_{x,i} = \tilde{\varepsilon}_{x,0,i} + \zeta_i \tilde{k}_{x,i} \qquad \tilde{\varepsilon}_{\theta,i} = \tilde{\varepsilon}_{\theta,0,i} + \zeta_i \tilde{k}_{\theta,i} \qquad \tilde{\gamma}_{x\theta,i} = \tilde{\gamma}_{x\theta,0,i} + \zeta_i \tilde{k}_{x\theta,i} \qquad i = 1,2 \tag{4}$$

where $\zeta_i = z_i/R_i$ is the dimensionless radial coordinate of the i-th cylindrical shell.

3. Anisotropic Elastic Shell Model for DWCNTs

Actually, CNTs are discrete systems composed of carbon atoms with covalent bonds, and therefore, they are intrinsically non-isotropic. Accordingly, it was proven that the use of an isotropic elastic shell model can lead to relevant errors in CNT vibration analysis, in particular to natural frequencies very different from those obtained by means of resonant Raman experimental spectroscopy or molecular dynamics numerical simulations, see Ref. [24]. On the basis of these findings, in the present paper, an anisotropic elastic shell model is adopted for DWCNT vibration analysis.

3.1. Stress–Strain Relationships

First of all, it should be stressed that the present study is conducted by assuming the plane stress hypothesis ($\sigma_z = 0$), which is peculiar to thin-walled structures.

In the case of anisotropic elastic material, the dimensionless stresses ($\tilde{\sigma}_{x,i}, \tilde{\sigma}_{\theta,i}, \tilde{\tau}_{x\theta,i}$) of the i-th cylindrical shell are related to the corresponding dimensionless strains by means of the following constitutive Equation [46]:

$$\begin{aligned} \tilde{\sigma}_{x,i} &= \tilde{Y}_{11,i}\tilde{\varepsilon}_{x,i} + \tilde{Y}_{12,i}\tilde{\varepsilon}_{\theta,i} + \tilde{Y}_{13,i}\tilde{\gamma}_{x\theta,i} \\ \tilde{\sigma}_{\theta,i} &= \tilde{Y}_{21,i}\tilde{\varepsilon}_{x,i} + \tilde{Y}_{22,i}\tilde{\varepsilon}_{\theta,i} + \tilde{Y}_{23,i}\tilde{\gamma}_{x\theta,i} \qquad i = 1,2 \\ \tilde{\tau}_{x\theta,i} &= \tilde{Y}_{31,i}\tilde{\varepsilon}_{x,i} + \tilde{Y}_{32,i}\tilde{\varepsilon}_{\theta,i} + \tilde{Y}_{33,i}\tilde{\gamma}_{x\theta,i} \end{aligned} \tag{5}$$

where the dimensionless material parameters $\tilde{Y}_{jk,i}$, which substitute Young's modulus and Poisson's ratio of the corresponding isotropic model, represent anisotropic surface elastic constants, in the form [46]:

$$\tilde{Y}_{jk,i} = \left(\tilde{G}_{lj,i}\tilde{G}_{lk,i} + 2\mu\tilde{H}_{lj,i}\tilde{H}_{lk,i}\right) \qquad j,k,l = 1,2,3 \text{ (sum over } l) \qquad i = 1,2 \tag{6}$$

which allow the chirality effects to be considered in the anisotropic elastic constitutive Equation (5), where ($\tilde{G}_{lj,i}, \tilde{G}_{lk,i}, \tilde{H}_{lj,i}, \tilde{H}_{lk,i}$) are dimensionless constants and μ is a dimensionless constant parameter [46]:

$$\mu = \frac{K_\theta}{K_\rho a^2} \tag{7}$$

where K_ρ and K_θ are force constants associated with the stretching and angular distortion of the carbon–carbon bond, respectively, which can be derived from molecular mechanics analyses or experimental data, see Ref. [23] for more details, and a is the carbon–carbon bond length.

The corresponding matrices $\widetilde{\mathbf{G}}_i$ and $\widetilde{\mathbf{H}}_i$ can be calculated as follows [46]:

$$\widetilde{\mathbf{G}}_i = \widetilde{\mathbf{B}}_i^{-1}\left(\tilde{\mathbf{I}} - \widetilde{\mathbf{D}}_i\tilde{\mathbf{F}}_i\right), \quad \widetilde{\mathbf{H}}_i = \widetilde{\mathbf{Q}}_i\tilde{\mathbf{F}}_i \qquad i = 1,2 \tag{8}$$

where $\tilde{\mathbf{I}}$ is the identity matrix, matrix $\tilde{\mathbf{F}}_i$ is given by [46]:

$$\tilde{\mathbf{F}}_i = \left[\widetilde{\mathbf{U}}_i\widetilde{\mathbf{B}}_i^{-1}\widetilde{\mathbf{D}}_i - (2\mu\widetilde{\mathbf{V}}_i\widetilde{\mathbf{A}}_i + \widetilde{\mathbf{W}}_i)\right]^{-1}\widetilde{\mathbf{U}}_i\widetilde{\mathbf{B}}_i^{-1} \qquad i = 1,2 \tag{9}$$

and matrices $\left(\widetilde{\mathbf{A}}_i, \widetilde{\mathbf{B}}_i, \widetilde{\mathbf{D}}_i, \widetilde{\mathbf{U}}_i, \widetilde{\mathbf{V}}_i, \widetilde{\mathbf{W}}_i, \widetilde{\mathbf{Q}}_i\right)$ are given by [46]:

$$\widetilde{\mathbf{A}}_i = \left\{\tilde{A}_{jk,i}\right\} = \left\{-\cos\omega_{jp,i}\cos\omega_{kp,i}\right\} \qquad j,k,p = 1,2,3 \text{ (sum over } p) \qquad i = 1,2 \tag{10}$$

$$\widetilde{\mathbf{B}}_i = \frac{1}{3\sqrt{r_i^2 + r_i s_i + s_i^2}} \begin{pmatrix} (2r_i + s_i)\cos\phi_{1,i} & -(r_i - s_i)\cos\phi_{2,i} & -(r_i + 2s_i)\cos\phi_{3,i} \\ \sqrt{3}\, s_i \sin\phi_{1,i} & -\sqrt{3}(r_i - s_i)\sin\phi_{2,i} & \sqrt{3}\, r_i \sin\phi_{3,i} \\ (2r_i + s_i)\sin\phi_{1,i} & -(r_i - s_i)\sin\phi_{2,i} & -(r_i + 2s_i)\sin\phi_{3,i} \end{pmatrix} \tag{11}$$

$$\widetilde{\mathbf{D}}_i = \frac{1}{3\sqrt{r_i^2 + r_i s_i + s_i^2}} \begin{pmatrix} -(2r_i + s_i)\sin\phi_{1,i} & (r_i - s_i)\sin\phi_{2,i} & (r_i + 2s_i)\sin\phi_{3,i} \\ \sqrt{3}\, s_i \cos\phi_{1,i} & -\sqrt{3}(r_i + s_i)\cos\phi_{2,i} & \sqrt{3}\, r_i \cos\phi_{3,i} \\ (2r_i + s_i)\cos\phi_{1,i} & -(r_i - s_i)\cos\phi_{2,i} & -(r_i + 2s_i)\cos\phi_{3,i} \end{pmatrix} \tag{12}$$

$$\widetilde{\mathbf{U}}_i = \begin{pmatrix} \sin\phi_{1,i} & \sin\phi_{2,i} & \sin\phi_{3,i} \\ \cos\phi_{1,i} & \cos\phi_{2,i} & \cos\phi_{3,i} \\ s_i\cos\phi_{1,i} & -(r_i + s_i)\cos\phi_{2,i} & r_i\cos\phi_{3,i} \end{pmatrix} \tag{13}$$

$$\widetilde{\mathbf{V}}_i = \begin{pmatrix} -\cos\phi_{1,i} & -\cos\phi_{2,i} & -\cos\phi_{3,i} \\ \sin\phi_{1,i} & \sin\phi_{2,i} & \sin\phi_{3,i} \\ 0 & 0 & 0 \end{pmatrix} \tag{14}$$

$$\widetilde{\mathbf{W}}_i = \begin{pmatrix} 0 & 0 & 0 \\ 0 & 0 & 0 \\ -s_i\sin\phi_{1,i} & (r_i + s_i)\sin\phi_{2,i} & -r_i\sin\phi_{3,i} \end{pmatrix} \tag{15}$$

$$\widetilde{\mathbf{Q}}_i = \left\{\tilde{Q}_{jk,i}\right\} = \left\{-\cos\omega_{kj,i}\right\} \qquad j,k = 1,2,3 \qquad i = 1,2 \tag{16}$$

where [46]:

$$\cos\omega_{jk,i} = \begin{cases} (\cos\phi_{j,i}\sin\phi_{p,i}\cos\varphi_{k,i} - \sin\phi_{j,i}\cos\phi_{p,i})/\sin\theta_{k,i} & j \neq k \neq p \\ 0 & j = k \end{cases} \tag{17}$$

and (r_i, s_i) are the chirality indices of the i-th carbon nanotube, which describe its rolling angle (i.e., direction), and therefore, define its radius by means of the formulation [18]:

$$R_i = \frac{\sqrt{3}\, a}{2\pi}\sqrt{r_i^2 + r_i s_i + s_i^2} \tag{18}$$

The structural parameters of the i-th SWCNT, i.e., chiral angles $(\phi_{1,i}, \phi_{2,i}, \phi_{3,i})$ and torsion angles $(\varphi_{1,i}, \varphi_{2,i}, \varphi_{3,i})$, which can be calculated by means of Equation [47]:

$$\phi_{1,i} = \arccos\frac{2r_i + s_i}{2\sqrt{r_i^2 + r_i s_i + s_i^2}} \qquad \phi_{2,i} = \frac{4\pi}{3} + \phi_{1,i} \qquad \phi_{3,i} = \frac{2\pi}{3} + \phi_{1,i} \tag{19}$$

$$\varphi_{1,i} = \frac{\pi}{\sqrt{r_i^2 + r_i s_i + s_i^2}}\cos\phi_{1,i} \qquad \varphi_{2,i} = \frac{\pi}{\sqrt{r_i^2 + r_i s_i + s_i^2}}\cos\left(\frac{\pi}{3} + \phi_{1,i}\right) \tag{20}$$

$$\varphi_{3,i} = \frac{\pi}{\sqrt{r_i^2 + r_i s_i + s_i^2}}\cos\left(\frac{\pi}{3} - \phi_{1,i}\right)$$

and bond angles $(\theta_{1,i}, \theta_{2,i}, \theta_{3,i})$, which are written in the following form [47]:

$$\cos\theta_{j,i} = \sin\phi_{k,i}\sin\phi_{p,i}\cos\varphi_{j,i} + \cos\phi_{k,i}\cos\phi_{p,i} \tag{21}$$

$$j,k,p = 1,2,3 \text{ (sum over } p) \qquad i = 1,2$$

are illustrated in Figure 2, see Ref. [22] for more details.

It should be stressed that the chirality of a generic SWCNT is indicated by the chiral angle ϕ_1, see Equation (19) and Figure 2. In particular, the two limiting cases of carbon nanotubes are $(r, 0)$, which gives chiral angle $\phi_1 = 0$ and is defined "zigzag" CNT, and (r, r), which gives chiral angle $\phi_1 = \pi/6$ and is defined "armchair" CNT. These two definitions are based on the different geometry of the carbon atoms along the circumferen-

tial direction of the nanotube. Moreover, zigzag and armchair CNTs are considered as achiral nanotubes, due to their high geometric symmetry, whereas SWCNTs with a chiral angle within the range $0 < \phi_1 < \pi/6$ are referred to as "chiral" CNTs, see Ref. [22] for details.

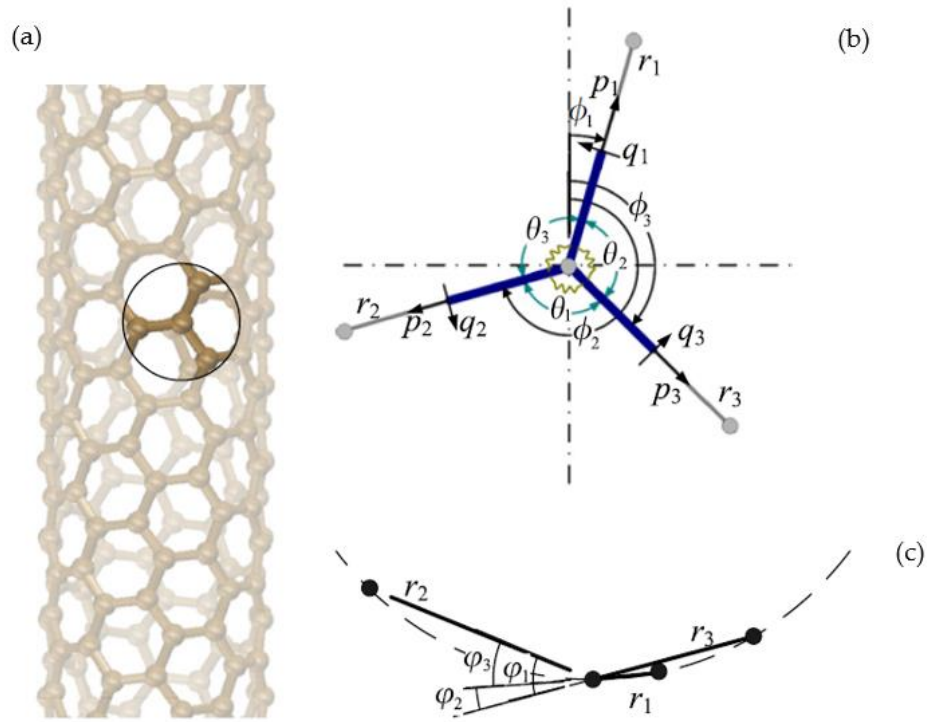

Figure 2. Schematic illustration of a (r, s) single-walled carbon nanotube. (**a**) Global structure with a zoom of a single representative atom; (**b**) side view of the local structure; (**c**) top view of the local structure. Reprinted with permission from Ref. [22], 2006, The Royal Society.

3.2. Force and Moment Resultants

Starting from the anisotropic elastic constitutive Equation (5), the corresponding dimensionless in-plane force resultants per unit length of the i-th shell $(\widetilde{N}_{x,i}, \widetilde{N}_{\theta,i}, \widetilde{N}_{x\theta,i})$ can be written as a function of the corresponding dimensionless middle surface strains and of the dimensionless material parameters $\tilde{Y}_{jk,i}$ in the form:

$$\begin{aligned}
\widetilde{N}_{x,i} &= \int_{-\beta_i/2}^{+\beta_i/2} \tilde{\sigma}_{x,i} d\zeta_i = \tilde{Y}_{11,i}\tilde{\varepsilon}_{x,0,i} + \tilde{Y}_{12,i}\tilde{\varepsilon}_{\theta,0,i} + \tilde{Y}_{13,i}\tilde{\gamma}_{x\theta,0,i} \\
\widetilde{N}_{\theta,i} &= \int_{-\beta_i/2}^{+\beta_i/2} \tilde{\sigma}_{\theta,i} d\zeta_i = \tilde{Y}_{21,i}\tilde{\varepsilon}_{x,0,i} + \tilde{Y}_{22,i}\tilde{\varepsilon}_{\theta,0,i} + \tilde{Y}_{23,i}\tilde{\gamma}_{x\theta,0,i} \\
\widetilde{N}_{x\theta,i} &= \int_{-\beta_i/2}^{+\beta_i/2} \tilde{\tau}_{x\theta,i} d\zeta_i = \tilde{Y}_{31,i}\tilde{\varepsilon}_{x,0,i} + \tilde{Y}_{32,i}\tilde{\varepsilon}_{\theta,0,i} + \tilde{Y}_{33,i}\tilde{\gamma}_{x\theta,0,i}
\end{aligned} \tag{22}$$

where $\beta_i = h/R_i$ is the thickness ratio of the i-th cylindrical shell.

Similarly, the dimensionless moment resultants per unit length of the i-th cylindrical shell $(\widetilde{M}_{x,i}, \widetilde{M}_{\theta,i}, \widetilde{M}_{x\theta,i})$ can be written as a function of the corresponding dimensionless middle surface changes in curvature and torsion and of the dimensionless material parameters $\tilde{Y}_{jk,i}$ in the form:

$$\widetilde{M}_{x,i} = \int_{-\beta_i/2}^{+\beta_i/2} \tilde{\sigma}_{x,i}\zeta_i d\zeta_i = \frac{\beta_i}{12}\left(\tilde{Y}_{11,i}\tilde{k}_{x,i} + \tilde{Y}_{12,i}\tilde{k}_{\theta,i} + \tilde{Y}_{13,i}\tilde{k}_{x\theta,i}\right)$$

$$\widetilde{M}_{\theta,i} = \int_{-\beta_i/2}^{+\beta_i/2} \tilde{\sigma}_{\theta,i}\zeta_i d\zeta_i = \frac{\beta_i}{12}\left(\tilde{Y}_{21,i}\tilde{k}_{x,i} + \tilde{Y}_{22,i}\tilde{k}_{\theta,i} + \tilde{Y}_{23,i}\tilde{k}_{x\theta,i}\right) \quad (23)$$

$$\widetilde{M}_{x\theta,i} = \int_{-\beta_i/2}^{+\beta_i/2} \tilde{\tau}_{x\theta,i}\zeta_i d\zeta_i = \frac{\beta_i}{12}\left(\tilde{Y}_{31,i}\tilde{k}_{x,i} + \tilde{Y}_{32,i}\tilde{k}_{\theta,i} + \tilde{Y}_{33,i}\tilde{k}_{x\theta,i}\right)$$

Finally, the dimensionless transverse shear forces per unit length of the i-th cylindrical shell ($\tilde{Q}_{x,i}, \tilde{Q}_{\theta,i}$), which are obtained directly from the expressions of the dimensionless moment resultants per unit length, can be written as:

$$\begin{aligned}
\tilde{Q}_{x,i} &= \frac{\beta_i^2}{12}\left(\alpha_i\left(\tilde{Y}_{11,i}\frac{\partial\tilde{k}_{x,i}}{\partial\eta} + \tilde{Y}_{12,i}\frac{\partial\tilde{k}_{\theta,i}}{\partial\eta} + \tilde{Y}_{13,i}\frac{\partial\tilde{k}_{x\theta,i}}{\partial\eta}\right) + \tilde{Y}_{31,i}\frac{\partial\tilde{k}_{x,i}}{\partial\theta} + \tilde{Y}_{32,i}\frac{\partial\tilde{k}_{\theta,i}}{\partial\theta} + \tilde{Y}_{33,i}\frac{\partial\tilde{k}_{x\theta,i}}{\partial\theta}\right) \\
\tilde{Q}_{\theta,i} &= \frac{\beta_i^2}{12}\left(\alpha_i\left(\tilde{Y}_{31,i}\frac{\partial\tilde{k}_{x,i}}{\partial\eta} + \tilde{Y}_{32,i}\frac{\partial\tilde{k}_{\theta,i}}{\partial\eta} + \tilde{Y}_{33,i}\frac{\partial\tilde{k}_{x\theta,i}}{\partial\eta}\right) + \tilde{Y}_{21,i}\frac{\partial\tilde{k}_{x,i}}{\partial\theta} + \tilde{Y}_{22,i}\frac{\partial\tilde{k}_{\theta,i}}{\partial\theta} + \tilde{Y}_{23,i}\frac{\partial\tilde{k}_{x\theta,i}}{\partial\theta}\right)
\end{aligned} \quad (24)$$

The previous equations will be used in the following in the expressions of the natural boundary conditions imposed on the i-th cylindrical shell, which involve forces and moments resultants.

3.3. Elastic Strain Energy

In the case of homogeneous, anisotropic and elastic material, assuming plane stress hypothesis ($\sigma_z = 0$), the dimensionless elastic strain energy $\widetilde{U}_i$ of the i-th cylindrical shell is expressed as a function of the dimensionless stresses ($\tilde{\sigma}_{x,i}, \tilde{\sigma}_{\theta,i}, \tilde{\tau}_{x\theta,i}$) and strains ($\tilde{\varepsilon}_{x,i}, \tilde{\varepsilon}_{\theta,i}, \tilde{\gamma}_{x\theta,i}$) as follows [44]:

$$\widetilde{U}_i = \frac{1}{2\beta_i}\int_0^1\int_0^{2\pi}\int_{-\beta_i/2}^{+\beta_i/2}\left(\tilde{\sigma}_{x,i}\tilde{\varepsilon}_{x,i} + \tilde{\sigma}_{\theta,i}\tilde{\varepsilon}_{\theta,i} + \tilde{\tau}_{x\theta,i}\tilde{\gamma}_{x\theta,i}\right)d\eta d\theta d\zeta \quad (25)$$

By inserting Equations (4) and (5) into Equation (25), the dimensionless elastic strain energy $\widetilde{U}_i$ can be rewritten as a function of the dimensionless middle surface strains ($\tilde{\varepsilon}_{x,0,i}, \tilde{\varepsilon}_{\theta,0,i}, \tilde{\gamma}_{x\theta,0,i}$) and changes in curvature and torsion ($\tilde{k}_{x,i}, \tilde{k}_{\theta,i}, \tilde{k}_{x\theta,i}$), and of the dimensionless material parameters $\tilde{Y}_{jk,i}$, and it becomes:

$$\begin{aligned}
\widetilde{U}_i = \frac{1}{2}\int_0^1\int_0^{2\pi}&\left(\tilde{Y}_{11,i}\tilde{\varepsilon}_{x,0,i}^2 + \tilde{Y}_{12,i}\tilde{\varepsilon}_{x,0,i}\tilde{\varepsilon}_{\theta,0,i} + \tilde{Y}_{13,i}\tilde{\varepsilon}_{x,0,i}\tilde{\gamma}_{x\theta,0,i} + \tilde{Y}_{21,i}\tilde{\varepsilon}_{x,0,i}\tilde{\varepsilon}_{\theta,0,i} + \right. \\
&\left. + \tilde{Y}_{22,i}\tilde{\varepsilon}_{\theta,0,i}^2 + \tilde{Y}_{23,i}\tilde{\varepsilon}_{\theta,0,i}\tilde{\gamma}_{x\theta,0,i} + \tilde{Y}_{31,i}\tilde{\varepsilon}_{x,0,i}\tilde{\gamma}_{x\theta,0,i} + \tilde{Y}_{32,i}\tilde{\varepsilon}_{\theta,0,i}\tilde{\gamma}_{x\theta,0,i} + \tilde{Y}_{33,i}\tilde{\gamma}_{x\theta,0,i}^2\right) \\
&d\eta d\theta + \frac{\beta_i^2}{24}\int_0^1\int_0^{2\pi}\left(\tilde{Y}_{11,i}\tilde{k}_{x,i}^2 + \tilde{Y}_{12,i}\tilde{k}_{x,i}\tilde{k}_{\theta,i} + \tilde{Y}_{13,i}\tilde{k}_{x,i}\tilde{k}_{x\theta,i} + \tilde{Y}_{21,i}\tilde{k}_{x,i}\tilde{k}_{\theta,i} + \right. \\
&\left. + \tilde{Y}_{22,i}\tilde{k}_{\theta,i}^2 + \tilde{Y}_{23,i}\tilde{k}_{\theta,i}\tilde{k}_{x\theta,i} + \tilde{Y}_{31,i}\tilde{k}_{x,i}\tilde{k}_{x\theta,i} + \tilde{Y}_{32,i}\tilde{k}_{\theta,i}\tilde{k}_{x\theta,i} + \tilde{Y}_{33,i}\tilde{k}_{x\theta,i}^2\right)d\eta d\theta
\end{aligned} \quad (26)$$

It should be observed that, in Equation (26), the first term on the right-hand side is associated to the middle surface strains of the shell, and therefore, it represents the stretching (tensile/compression) energy, while the second term is associated to the middle surface changes in curvature and torsion of the shell, and therefore it represents the bending (flexural) energy [18].

The dimensionless elastic strain energy of a DWCNT is given by [44]:

$$\widetilde{U} = \sum_{i=1}^{2}\delta_i\widetilde{U}_i \quad (27)$$

where $\delta_i = R_i/R_1$ and R_1 is the radius of the inner SWCNT.

3.4. Kinetic Energy

The most important issue in the determination of the dimensionless kinetic energy is the definition of the dimensionless time variable. In the present work, the dimensionless time variable τ is obtained by introducing the reference dimensional circular frequency ω_0, in the form:

$$\tau = \omega_0 t \qquad \omega_0 = \sqrt{\frac{Y}{\rho_m h R_1^2}} \tag{28}$$

where t is the corresponding dimensional time variable, ρ_m is the mass density of the material and

$$Y = \frac{2K_\rho}{3\sqrt{3}} \tag{29}$$

is a reference dimensional surface elastic constant.

Starting from the definition of dimensionless time variable τ (28), the dimensionless velocity field of the i-th cylindrical shell $(\tilde{u}_i', \tilde{v}_i', \tilde{w}_i')$ is written as [44]:

$$\tilde{u}_i' = \frac{d\tilde{u}_i}{d\tau} = \frac{\dot{u}_i}{R_i\omega_0} \qquad \tilde{v}_i' = \frac{d\tilde{v}_i}{d\tau} = \frac{\dot{v}_i}{R_i\omega_0} \qquad \tilde{w}_i' = \frac{d\tilde{w}_i}{d\tau} = \frac{\dot{w}_i}{R_i\omega_0} \qquad i = 1,2 \tag{30}$$

where $(\dot{u}_i, \dot{v}_i, \dot{w}_i)$ is the corresponding dimensional velocity field.

Neglecting the rotary inertia effect, the dimensionless kinetic energy of the i-th cylindrical shell is given by [44]:

$$\tilde{T}_i = \frac{1}{2}\delta_i^2 \int_0^1 \int_0^{2\pi} (\tilde{u}_i'^2 + \tilde{v}_i'^2 + \tilde{w}_i'^2) d\eta d\theta \qquad i = 1,2 \tag{31}$$

It can be noted that, differently from the elastic strain energy (26), the kinetic energy (31) does not depend on the material properties, as the dimensionless material parameters $\tilde{Y}_{jk,i}$ are not present and the mass density ρ_m is included in the definition of the reference circular frequency ω_0), and therefore, it assumes the same expression for both isotropic and anisotropic elastic material.

The dimensionless kinetic energy of a DWCNT is given by [44]:

$$\tilde{T} = \sum_{i=1}^{2} \delta_i \tilde{T}_i \tag{32}$$

3.5. Van der Waals interaction forces

In the present paper, the actual discrete DWCNT is modelled by means of a couple of concentric equivalents continuous thin cylindrical shells, and van der Waals interaction energy potential between the two layers can be estimated by the Lennard–Jones model [30]:

$$V_{LJ}(a) = 4\varepsilon\left(\left(\frac{\sigma}{a}\right)^{12} - \left(\frac{\sigma}{a}\right)^{6}\right) \tag{33}$$

where ε is the carbon–carbon potential depth, σ is the carbon–carbon equilibrium separation distance and a is the carbon–carbon bond length (i.e., the distance between the interacting atoms).

The van der Waals interaction force is obtained by deriving Lennard–Jones pair potential (33), with respect to the carbon–carbon bond length [41]:

$$F(a) = -\frac{dV_{LJ}(a)}{da} = \frac{24\varepsilon}{\sigma}\left(2\left(\frac{\sigma}{a}\right)^{13} - \left(\frac{\sigma}{a}\right)^{7}\right) \tag{34}$$

where the negative value represents the attractive force between a pair of atoms, whereas the positive value represents the corresponding repulsive force.

Since only the infinitesimal buckling of CNTs is of interest, then the van der Waals force (34) can be estimated via the Taylor expansion to the first order around the equilibrium position prior to buckling, in the form [41]:

$$F(a) = F(a_0) + \frac{dF(a_0)}{da_0}(a - a_0) \tag{35}$$

where a_0 is the initial carbon–carbon atom distance of the two layers prior to bucking.

By substituting Equation (34) into expansion (35), it is derived [41]:

$$F(a) = \frac{24\varepsilon}{\sigma}\left(2\left(\frac{\sigma}{a_0}\right)^{13} - \left(\frac{\sigma}{a_0}\right)^{7}\right) - \frac{24\varepsilon}{\sigma^2}\left(26\left(\frac{\sigma}{a_0}\right)^{14} - 7\left(\frac{\sigma}{a_0}\right)^{8}\right)(a - a_0) \quad (36)$$

At the equilibrium position prior to buckling, the initial van der Waals interaction force $F(a_0)$ is very small, and therefore, can be neglected.

By integrating Equation (36) over the entire DWCNT, it is obtained the pressure p_i exerted on the ith SWCNT due to the van der Waals interactions between the layers (i, j), expressed as a function of the radial displacements (w_i, w_j) [41]:

$$p_i(\eta, \theta) = c_{ij}(w_i - w_j) \qquad i, j = 1,2 \qquad i \neq j \quad (37)$$

where c_{ij} is the van der Waals interaction coefficient between the layers (i, j).

In the literature, several formulations for the van der Waals interaction coefficient are reported; in particular, it can be expressed by adopting Ru's and He's formulations.

3.5.1. Van der Waals Interaction Coefficient: Ru's Formulation

In Ru's formulation, the van der Waals interaction coefficient between the two layers is estimated starting from the energy potential per unit area between a carbon atom and a flat graphite sheet, as reported by Girifalco and Lad [34], and it is expressed in the form [31]:

$$c_{Ru} = -\frac{3.2 \times 10^2 \text{ erg/cm}^2}{0.16a^2} \quad (38)$$

where $1 \text{ erg/cm}^2 = 10^{-3} \text{ N/m}$.

Note that the equilibrium distance between a carbon atom and a flat graphite sheet is around 0.34 nm [34], so the initial pressure between the inner and outer tubes is zero if the initial interlayer spacing is 0.34 nm. In this case, any increase (decrease) in the interlayer spacing causes an attractive (repulsive) van der Waals interaction, and then coefficient c should be negative (positive) [32].

From expression (38), it can be observed that, in Ru's formulation, the van der Waals interaction coefficient represents a constant parameter, which is assumed to depend on the distance between the interacting atoms a, while it is not dependent on CNT diameter. Specifically, the curvature effect has been ignored because it is usually small for the MWNTs of the larger innermost radius [5–7].

3.5.2. Van der Waals Interaction Coefficient: He's Formulation

In He's formulation, the van der Waals interaction coefficient is derived via the direct integration of Equation (36), and it is expressed in the form [41]:

$$c_{ij,He} = -\left(\frac{1001\pi\varepsilon\sigma^{12}}{3a^4}E_{ij}^{13} - \frac{1120\pi\varepsilon\sigma^{6}}{9a^4}E_{ij}^{7}\right)R_j \qquad i, j = 1,2 \qquad i \neq j \quad (39)$$

From expression (39), it can be observed that, in He's formulation, the van der Waals interaction coefficient depends on the radius R_j of the jth layer. In addition, for a specific DWCNT geometry, it is obtained that $c_{ij} \neq c_{ji}$, i.e., the two coefficients are different, with the relationship $c_{ij}R_i = c_{ji}R_j$.

The elliptical integral E_{ij}^m of expression (39) is written as [41]:

$$E_{ij}^m = (R_j + R_i)^{-m}\int_0^{\pi/2}\frac{d\theta}{(1 - k_{ij}\cos^2\theta)^{m/2}} \qquad i, j = 1,2 \qquad i \neq j \qquad m = 7,13 \quad (40)$$

and the geometric coefficient k_{ij} of Equation (40) is written as [41]:

$$k_{ij} = \frac{4R_jR_i}{(R_j + R_i)^2} \qquad i, j = 1,2 \qquad i \neq j \quad (41)$$

3.5.3. Van der Waals Interaction Energy

The van der Waals interaction energy of the i-th cylindrical shell, which models the SWCNT, is expressed in dimensionless form as follows [44]:

$$\tilde{V}_i = -\frac{1}{2}\delta_i \int_0^1 \int_0^{2\pi} \tilde{p}_i(\eta,\theta)\tilde{w}_i d\eta d\theta \qquad i = 1,2 \tag{42}$$

The dimensionless van der Waals interaction energy of a DWCNT is given by [44]:

$$\tilde{V} = \sum_{i=1}^{2} \delta_i \tilde{V}_i \tag{43}$$

4. Vibration Modelling of DWCNTs

In the case of DWCNTs, a modal vibration can be formally written in terms of the three dimensionless displacements of the i-th cylindrical shell $(\tilde{u}_i, \tilde{v}_i, \tilde{w}_i)$ as [44]:

$$\tilde{u}_i(\eta,\theta,\tau) = \widetilde{U}_i(\eta,\theta)\tilde{f}_i(\tau) \qquad \tilde{v}_i(\eta,\theta,\tau) = \widetilde{V}_i(\eta,\theta)\tilde{f}_i(\tau) \qquad \tilde{w}_i(\eta,\theta,\tau) = \widetilde{W}_i(\eta,\theta)\tilde{f}_i(\tau) \qquad i = 1,2 \tag{44}$$

where $(\widetilde{U}_i, \widetilde{V}_i, \widetilde{W}_i)$ are the corresponding three dimensionless components of the modal shape and $\tilde{f}_i(\tau)$ is the corresponding dimensionless time law, which is supposed to be the same for the three different displacements (i.e., synchronous motion hypothesis).

The three modal shape components $(\widetilde{U}_i, \widetilde{V}_i, \widetilde{W}_i)$ can be expressed in different ways. Usually, they are expanded by means of a double series in terms of harmonic functions along the longitudinal and circumferential directions, see for example Ref. [35]. In the present work, they are expanded by means of a double mixed series in terms of m-th degree Chebyshev orthogonal polynomials $T_m^*(\eta) = T_m(2\eta - 1)$ along the longitudinal direction η and harmonic functions $(\cos n\theta\,, \sin n\theta)$ along the circumferential direction θ [44]:

$$\widetilde{U}_i(\eta,\theta) = \sum_{m=0}^{M_u}\sum_{n=0}^{N} \widetilde{U}_{i,m,n} T_m^*(\eta)\cos n\theta \qquad \widetilde{V}_i(\eta,\theta) = \sum_{m=0}^{M_v}\sum_{n=0}^{N} \widetilde{V}_{i,m,n} T_m^*(\eta)\sin n\theta$$
$$\widetilde{W}_i(\eta,\theta) = \sum_{m=0}^{M_w}\sum_{n=0}^{N} \widetilde{W}_{i,m,n} T_m^*(\eta)\cos n\theta \qquad i = 1,2 \tag{45}$$

where m is the number of longitudinal half-waves (maximum values (M_u, M_v, M_w)), n is the number of circumferential waves (maximum value N) and $(\widetilde{U}_{i,m,n}, \widetilde{V}_{i,m,n}, \widetilde{W}_{i,m,n})$ are unknown coefficients, which can be obtained by imposing the boundary conditions.

This last is the most relevant difference due to the choice of Chebyshev polynomials instead of harmonic functions to model DWCNT vibrations along the longitudinal direction; actually, the boundary conditions are automatically satisfied by harmonic functions, while they are not automatically satisfied by Chebyshev polynomials, and therefore, in the second approach, they must be imposed on the unknown coefficients $(\widetilde{U}_{i,m,n}, \widetilde{V}_{i,m,n}, \widetilde{W}_{i,m,n})$, as in the present work.

4.1. Boundary Conditions

In this paper, simply supported DWCNTs are considered. The corresponding boundary conditions on the two ends of the two SWCNTs are expressed in the form [45]:

$$\tilde{v}_i(\eta,\theta) = 0 \qquad \tilde{w}_i(\eta,\theta) = 0 \qquad \widetilde{N}_{x,i}(\eta,\theta) = 0 \qquad \widetilde{M}_{x,i}(\eta,\theta) = 0 \qquad \eta = 0,1 \qquad i = 1,2 \tag{46}$$

which represent both geometric (on the displacements $(\tilde{v}_i, \tilde{w}_i)$) and natural (on the force $\widetilde{N}_{x,i}$ and moment $\widetilde{M}_{x,i}$ resultants) conditions, where the dependency on the dimensionless time variable τ is not taken into account (modal vibration analysis).

By taking into account Equations (22) and (23) for the dimensionless force and moment resultants, the two natural boundary conditions (46) can be rewritten as a function

of the dimensionless middle surface strains and changes in curvature and torsion of the i-th cylindrical shell in the following form:

$$\widetilde{N}_{x,i}(\eta,\theta) = \tilde{Y}_{11,i}\tilde{\varepsilon}_{x,0,i} + \tilde{Y}_{12,i}\tilde{\varepsilon}_{\theta,0,i} + \tilde{Y}_{13,i}\tilde{\gamma}_{x\theta,0,i} = 0$$

$$\widetilde{M}_{x,i}(\eta,\theta) = \frac{\beta_i}{12}\left(\tilde{Y}_{11,i}\tilde{k}_{x,i} + \tilde{Y}_{12,i}\tilde{k}_{\theta,i} + \tilde{Y}_{13,i}\tilde{k}_{x\theta,i}\right) = 0 \qquad \eta = 0,1 \quad i = 1,2 \qquad (47)$$

Since the boundary conditions are related only to the dimensionless longitudinal coordinate η and do not depend on the circumferential coordinate θ (i.e., they are axisymmetric), then in the expressions (47) of the dimensionless force and moment resultants only the dimensionless middle surface strain and change in curvature along the longitudinal direction must be considered, and therefore, expressions (47) become:

$$\widetilde{N}_{x,i}(\eta) = \tilde{Y}_{11,i}\tilde{\varepsilon}_{x,0,i} = \tilde{Y}_{11,i}\alpha_i\frac{\partial\tilde{u}_i}{\partial\eta} = 0$$

$$\widetilde{M}_{x,i}(\eta) = \frac{\beta_i}{12}\tilde{Y}_{11,i}\tilde{k}_{x,i} = -\frac{\beta_i}{12}\tilde{Y}_{11,i}\alpha_i^2\frac{\partial^2\widetilde{w}_i}{\partial\eta^2} = 0 \qquad \eta = 0,1 \quad i = 1,2 \qquad (48)$$

Starting from the expressions for the geometric boundary conditions (46) and the natural boundary conditions (48), the following equations in terms of the dimensionless displacements $(\tilde{u}_i, \tilde{v}_i, \widetilde{w}_i)$ related to the longitudinal coordinate η of the i-th cylindrical shell are derived:

$$\tilde{v}_i(\eta) = 0 \qquad \widetilde{w}_i(\eta) = 0 \qquad \frac{\partial\tilde{u}_i}{\partial\eta}(\eta) = 0 \qquad \frac{\partial^2\widetilde{w}_i}{\partial\eta^2}(\eta) = 0 \qquad \eta = 0,1 \qquad i = 1,2 \qquad (49)$$

By substituting expressions (49) into Equations (44) for the dimensionless displacements, the following conditions in terms of expansions (45) for the corresponding modal shape components are derived [45]:

$$\tilde{V}_i(\eta) = \sum_{m=0}^{M_v}\tilde{V}_{i,m,n}T_m^*(\eta) = 0$$

$$\widetilde{W}_i(\eta) = \sum_{m=0}^{M_w}\widetilde{W}_{i,m,n}T_m^*(\eta) = 0$$

$$\widetilde{U}_{i,\eta}(\eta) = \sum_{m=0}^{M_u}\widetilde{U}_{i,m,n}T_{m,\eta}^*(\eta) = 0 \qquad \eta = 0,1 \quad i = 1,2 \qquad (50)$$

$$\widetilde{W}_{i,\eta\eta}(\eta) = \sum_{m=0}^{M_w}\widetilde{W}_{i,m,n}T_{m,\eta\eta}^*(\eta) = 0$$

where $(\cdot)_{,\eta} = \partial(\cdot)/\partial\eta$ and $(\cdot)_{,\eta\eta} = \partial^2(\cdot)/\partial\eta^2$.

The linear algebraic system given by Equation (50) can then be solved analytically in terms of the coefficients $(\widetilde{U}_{i,1,n}, \widetilde{U}_{i,2,n}, \tilde{V}_{i,0,n}, \tilde{V}_{i,1,n}, \widetilde{W}_{i,0,n}, \widetilde{W}_{i,1,n}, \widetilde{W}_{i,2,n}, \widetilde{W}_{i,3,n})$, for $n \in [0, N]$. Therefore, in the specific case of simply supported DWCNTs, eight different dimensionless coefficients for each SWCNT are obtained.

4.2. Rayleigh–Ritz Method

In the case of DWCNTs, the maximum number of variables needed to properly describe a generic vibration mode (m, n), with m longitudinal half-waves and n circumferential waves, is given by $N_p = 2 \times (M_u + M_v + M_w + 3 - p)$, where 2 is the number of concentric SWCNTs, $M_u = M_v = M_w$ is the maximum number of longitudinal half-waves considered and p is the number of equations needed to satisfy the boundary conditions:

as previously demonstrated, in the case of DWCNTs with simply supported boundary conditions it is imposed $p = 8$.

A convergence analysis was performed in order to obtain the correct order of Chebyshev orthogonal polynomials (i.e., the maximum number of longitudinal half-waves) to be adopted: since it was obtained that $M_u = M_v = M_w = 11$ allows the modal shapes with a number of longitudinal half-waves until $m = 5$ to be correctly modelled, and $m = 5$ is the maximum number of longitudinal half-waves considered in the numerical analyses of the present work, then $M_u = M_v = M_w = 11$ provides accurate results with relatively reduced computational effort.

For a multi-mode analysis including different values of circumferential waves n, the number of degrees of freedom of the mechanical system is given by $N_{\max} = N_p \times (N + 1)$, where N is the maximum number of circumferential waves considered.

Equations (44) are inserted in the expressions of elastic strain energy (26), kinetic energy (31) and van der Waals interaction energy (42) in order to calculate the value of Rayleigh quotient $R(\tilde{\mathbf{q}})$, where $\tilde{\mathbf{q}}$ is a vector containing all the unknown coefficients of expansions (45), expressed as [46]:

$$\tilde{\mathbf{q}} = \begin{bmatrix} \vdots \\ \widetilde{U}_{i,m,n} \\ \widetilde{V}_{i,m,n} \\ \widetilde{W}_{i,m,n} \\ \vdots \end{bmatrix} \qquad i = 1,2 \tag{51}$$

After imposing the stationarity on the Rayleigh quotient, the following classic eigenvalue problem in dimensionless form is obtained [46]:

$$\left(-\tilde{\omega}^2\tilde{\mathbf{M}} + \tilde{\mathbf{K}}\right)\tilde{\mathbf{q}} = \mathbf{0} \tag{52}$$

which provides approximate dimensionless circular frequencies (eigenvalues $\tilde{\omega}_j$) and modal shapes (eigenvectors $\tilde{\mathbf{q}}_j$), with $j = (1,2,\dots,N_{\max})$, where $\tilde{\mathbf{M}}$ and $\tilde{\mathbf{K}}$ are the dimensionless mass and stiffness matrices, respectively.

The approximate modal shape of the j-th mode of the i-th shell is provided by the expansions (45), where coefficients $(\widetilde{U}_{i,m,n}, \widetilde{V}_{i,m,n}, \widetilde{W}_{i,m,n})$ are replaced with coefficients $(\widetilde{U}^{(j)}_{i,m,n}, \widetilde{V}^{(j)}_{i,m,n}, \widetilde{W}^{(j)}_{i,m,n})$, which are the components of the j-th eigenvector $\tilde{\mathbf{q}}$ of Equation (52), and the vector function [47]:

$$\tilde{\mathbf{W}}^{(j)}(\eta,\theta) = \begin{bmatrix} \widetilde{U}_i^{(j)}(\eta,\theta) \\ \widetilde{V}_i^{(j)}(\eta,\theta) \\ \widetilde{W}_i^{(j)}(\eta,\theta) \end{bmatrix} \qquad i = 1,2 \tag{53}$$

is the approximation of the j-th eigenfunction vector of the original problem.

Finally, it must be underlined that, in order to obtain the corresponding dimensional natural frequencies f_j of DWCNTs, the dimensionless circular frequencies (eigenvalues) $\tilde{\omega}_j$ have to be multiplied by the dimensional constant term $\omega_0/2\pi$ (with dimensions s^{-1}).

5. Numerical Results

In the present work, natural frequencies of DWCNTs obtained via Ru's (38) and He's (39) formulations of the van der Waals interaction coefficient between the two concentric SWCNTs are compared. The Donnell shell theory is applied to obtain strain-displacement relationships. An anisotropic elastic shell model is adopted to take into account the chirality effects of CNTs. Simply supported boundary conditions are considered. Vibration modes with different numbers of waves along the longitudinal and circumferential directions are analysed. DWCNTs with different values of diameters are investigated.

In Table 1, the values of carbon–carbon (C-C) bond parameters (a, k_ρ, k_θ), C-C distance parameters (ε, σ) and CNT equivalent parameters (h, ρ_m), retrieved from the pertinent literature, are reported.

In particular, parameters k_ρ and k_θ, which denote force constants related to the variance of C-C bond length a and angle θ, respectively, and are used in the present work to compute the anisotropic elastic properties of CNTs, were derived in the molecular mechanics "stick-spiral model" developed by Chang et al. [22].

Moreover, parameters ε and σ, which denote C-C potential depth and equilibrium distance, respectively, and are used in this work to simulate the van der Waals interaction forces, were determined by He et al. [41] via buckling analysis of MWCNTs.

Finally, parameter h, which represents CNT equivalent thickness, and is adopted in the present analysis to study the actual discrete DWCNT as a couple of concentric equivalent continuous cylindrical shells, was derived from MD simulations of CNT energy by Yakobson et al. [14].

Table 1. Mechanical parameters adopted in the anisotropic elastic shell model.

C-C Bond Parameters	
C-C bond length a (nm)	0.142
C-C bond elongation K_ρ (nN/nm)	742
C-C bond angle variance K_θ (nN · nm)	1.42
C-C distance parameters	
C-C potential depth ε (10^{-22} J)	4.755
C-C equilibrium separation distance σ (nm)	0.3407
CNT equivalent parameters	
Thickness h (nm)	0.066
Mass density ρ_m (kg/m^3)	11700

5.1. Validation of the Proposed Model in the Isotropic Case

In order to justify the validity of the proposed model, let us consider the corresponding isotropic case, in which the SWCNT is assumed to be an isotropic elastic thin shell, with tensile rigidity C (in-plane stiffness), bending rigidity D (flexural stiffness), surface density ρ_s (mass density ρ_m per unit lateral area h) and Poisson's ratio ν reported in Table 2, where chirality effects are neglected, see Ref. [14] for more details.

Table 2. Mechanical parameters adopted in the isotropic elastic shell model.

Tensile rigidity C (J/m^2)	360
Bending rigidity D (J)	1.362×10^{-19}
Surface density ρ_s (kg/m^2)	7.718×10^{-7}
Poisson's ratio ν	0.19

To this purpose, in this Section, the results of the present elastic shell model in isotropic form, which considers Chebyshev orthogonal polynomials along the longitudinal direction and harmonic functions along the circumferential direction, are compared with the ones of the isotropic elastic shell models of Refs. [35,42], which adopt harmonic functions along both longitudinal and circumferential directions, and use Ru's and He's formulations for van der Waals interaction coefficient, respectively.

This check is important because there can be relevant differences between the results due to the different shape functions used in the modal expansions of the displacement field, and the accuracy of the natural frequencies depends strongly on the choice of modal shape functions. Moreover, it must be stressed that, in order to perform a correct analysis, the same thin shell theory, i.e., the Donnell shell theory, is adopted.

In Tables 3 and 4, the natural frequencies of a simply supported DWCNT with inner radius $R_1 = 5$ nm and aspect ratio $L/R_2 = 10$ are reported. The Donnell shell theory and isotropic elastic shell model are adopted. The van der Waals interaction coefficient is expressed via Ru's (Table 3) and He's (Table 4) formulations. Circumferential flexure

modes ($n = 2$) are analysed. Comparisons between present and Ref. [35] models (see Table 3), and present and Ref. [42] models (see Table 4), are performed.

From Tables 3 and 4, it is observed that the present elastic shell model in isotropic form is accurate both for Ru's and for He's formulations, as it gives natural frequencies with less than 1% difference, and therefore, the validity of the shape functions adopted in the modal expansions of the displacement field is confirmed.

Table 3. Natural frequencies (THz) of a simply supported DWCNT with innermost radius R_1 = 5 nm and aspect ratio L/R_2 = 10. Donnell shell theory. Isotropic elastic shell model. Van der Waals interaction coefficient expressed on the basis of Ru's formulation. Circumferential flexure modes (n = 2). Comparisons between present and Ref. [35] models.

	Natural Frequency (THz)				Diff. (%)
Mode (m,n)	**Prevalent Displacement**	**Prevalent Mode Shape**	**Present Model (Ru)**	**Ref. [35] Model (Ru)**	
(1,2)	w	R_1	0.0163	0.0162	0.62
(2,2)	w	R_1	0.0511	0.0509	0.39
(3,2)	w	R_1	0.1025	0.1020	0.49
(1,2)	u	R_2	0.8508	0.8438	0.83
(2,2)	u	R_2	0.8850	0.8775	0.85
(1,2)	u	R_1	0.9070	0.8999	0.79
(3,2)	u	R_2	0.9334	0.9254	0.86
(2,2)	u	R_1	0.9446	0.9375	0.76
(3,2)	u	R_1	1.0050	0.9977	0.73
(1,2)	v	R_2	1.3114	1.3080	0.26
(2,2)	v	R_2	1.3601	1.3567	0.25
(3,2)	v	R_2	1.4371	1.4334	0.26
(1,2)	v	R_1	1.5384	1.5371	0.08
(2,2)	v	R_1	1.5692	1.5679	0.08
(3,2)	v	R_1	1.6214	1.6201	0.08
(1,2)	w	R_1	2.7006	2.7000	0.02
(2,2)	w	R_1	2.7011	2.7005	0.02
(3,2)	w	R_1	2.7021	2.7015	0.02

Table 4. Natural frequencies (THz) of a simply supported DWCNT with innermost radius R_1 = 5 nm and aspect ratio L/R_2 = 10. Donnell shell theory. Isotropic elastic shell model. Van der Waals interaction coefficient expressed on the basis of He's formulation. Circumferential flexure modes (n = 2). Comparisons between present and Ref. [42] models.

	Natural Frequency (THz)				Diff. (%)
Mode (m,n)	**Prevalent Displacement**	**Prevalent Mode Shape**	**Present Model (He)**	**Ref. [42] Model (He)**	
(1,2)	w	R_1	0.0163	0.0163	0.00
(2,2)	w	R_1	0.0511	0.0509	0.39
(3,2)	w	R_1	0.1025	0.1021	0.39
(1,2)	u	R_2	0.8508	0.8440	0.81
(2,2)	u	R_2	0.8852	0.8782	0.80
(1,2)	u	R_1	0.9071	0.8998	0.81
(3,2)	u	R_2	0.9339	0.9266	0.79
(2,2)	u	R_1	0.9447	0.9372	0.80
(3,2)	u	R_1	1.0052	0.9972	0.80
(1,2)	v	R_2	1.3157	1.3130	0.21

(2,2)	v	R_2	1.3642	1.3620	0.16
(3,2)	v	R_2	1.4409	1.4380	0.20
(1,2)	v	R_1	1.5387	1.5360	0.18
(2,2)	v	R_1	1.5696	1.5670	0.17
(3,2)	v	R_1	1.6218	1.6190	0.17
(1,2)	w	R_1	2.7831	2.7830	0.00
(2,2)	w	R_1	2.7835	2.7840	0.02
(3,2)	w	R_1	2.7843	2.7840	0.01

5.2. Ru's vs He's Formulations of the van der Waals Interaction Coefficient for DWCNTs

Before comparing the natural frequencies of DWCNTs obtained by considering an anisotropic elastic shell model via Ru's and He's formulations, it is useful to investigate the values of the corresponding interaction coefficients under different values of CNT diameter, in order to justify the assumption of He's formulation as a reference in the comparisons.

In Figure 3, the effect of the DWCNT inner radius R_1 on the value of the van der Waals interaction coefficient c obtained by assuming the C-C bond parameters (a, ε, σ) of Table 1 and considering Ru's (38) and He's (39) formulations is shown.

From this Figure, it can be observed that, for a very large inner radius ($R_1 > 10$ nm), the two different interaction coefficients c_{12} and c_{21} deriving from He's formulation tend asymptotically to the same value ($c \approx 1.09$). This is due to the fact that as the inner radius increases, the outer radius also increases, while the distance between the two layers remains constant; therefore, the percentage difference between the inner and outer radius decreases, and the values of the two coefficients converge.

Moreover, it can be observed that this value is quite close to the constant one assumed by the interaction coefficient from Ru's formulation ($c \approx 1$). This is because, for a sufficiently large inner radius, the interaction coefficient no longer depends on the radius, but it assumes a constant value, which is similar to Ru's and He's formulations.

This behaviour, however, is not important for the modelling of CNTs, since it lies outside the range commonly assumed for the radius of CNTs. In fact, it is reported that "a single-wall nanotube is defined by a cylindrical graphene sheet with a diameter of about 0.7–10.0 nm, though most of the observed single-wall nanotubes have diameters <2 nm", see Ref. [24]. For this reason, it is important to focus the attention on the comparison between the interaction coefficients, and the corresponding natural frequencies of DWCNTs, from Ru's and He's formulations in this range of inner radius.

From Figure 3 it can be observed that, for a sufficiently small inner radius ($R_1 < 1$ nm), such as commonly assumed by CNTs, the two interaction coefficients c_{12} and c_{21} from He's formulation have very different values. This is because, in this range, the distance between the layers is significant with respect to the relative radii; therefore, the percentage difference between the inner and outer radius is very high, and the values of the two interaction coefficients diverge.

Moreover, it can be observed that these two values are very different compared to the constant one assumed by the interaction coefficient derived from Ru's formulation. This is due to the fact that, for a sufficiently small inner radius, the interaction coefficient strongly depends on the radius itself, and therefore it assumes very distant values for Ru's and He's formulations.

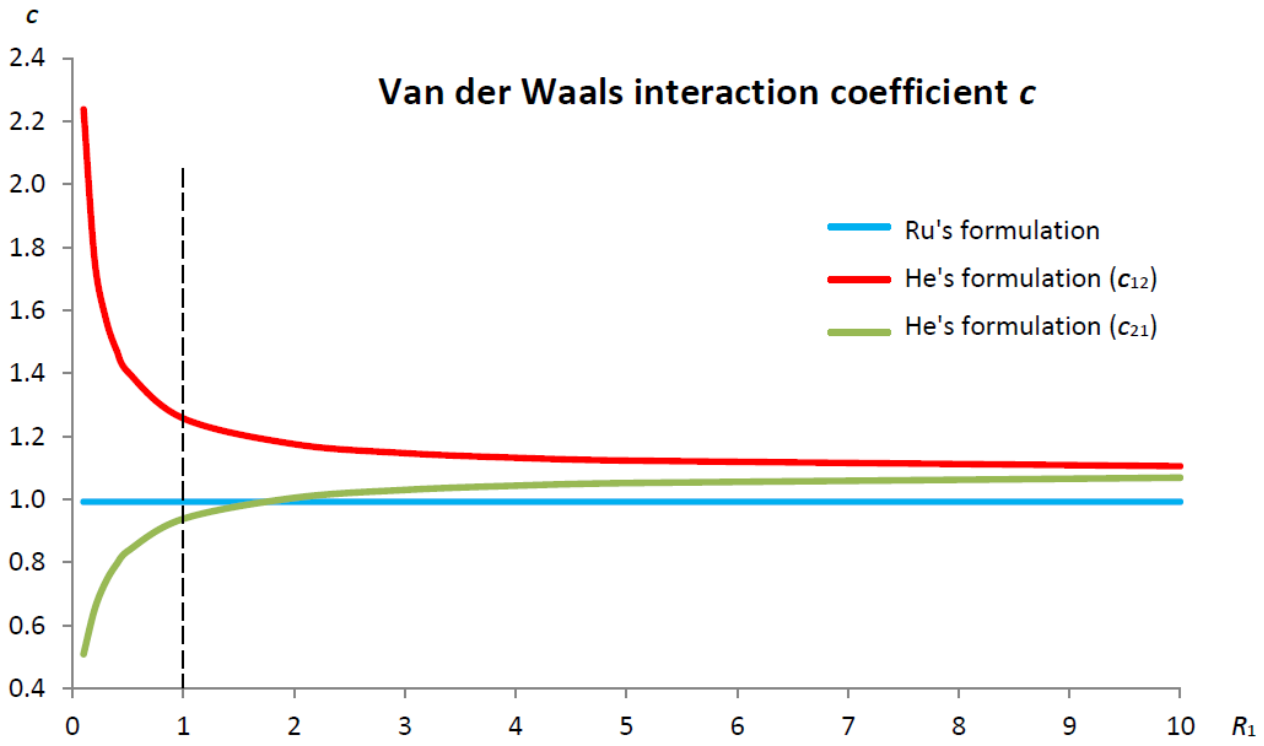

Figure 3. Effect of the inner radius R_1 (10^{-9} m) on the value of van der Waals interaction coefficient c (10^{20} N/m^3) of the DWCNT of Table 1. Comparison between Ru's (38) and He's (39) formulations.

As stated above, He's formulation, with respect to Ru's one, taking into account the effect of CNT diameter on the value of the van der Waals interaction coefficient, is able to simulate more correctly the actual CNT behaviour, which is anisotropic, that is the elastic properties of the material depend on CNT chirality and size, and therefore is more accurate.

This is especially true for a relatively small CNT diameter (< 2 nm), where it is known from the literature that the surface elastic constants assume values that strongly depend on chirality and size, and therefore it is necessary to adopt an anisotropic elastic model. On the other hand, the surface elastic constants tend asymptotically to constant values coinciding with those of the relative constants of graphite as CNT diameter increases, and therefore it is possible to adopt an isotropic elastic model, see Ref. [25] for more details.

In order to take into account chirality and size effects of CNTs, in the following, an anisotropic elastic shell model will be used to obtain the natural frequencies of DWCNTs. Moreover, since He's formulation is able to simulate more properly the actual anisotropic behaviour of CNTs, then in the following, it will be used as a reference to investigate the applicability and limitations of Ru's formulation for vibration modelling of DWCNTs.

5.3. Applicability and Limitations of Ru's Formulation for DWCNTs

In the present Section, starting from the previously reported results, natural frequencies of DWCNTs obtained via Ru's and He's formulations of the van der Waals interaction coefficient between the layers are compared. The Donnell shell theory and anisotropic elastic shell model are applied. Different values of diameters and wavenumbers along the longitudinal and circumferential directions are considered.

In Table 5, comparisons between the natural frequencies of the simply supported DWCNT of Table 1 with inner radius $R_1 = 5$ nm and aspect ratio $L/R_2 = 10$ are shown. Circumferential flexure modes ($n = 2$) are analysed. The number of longitudinal half-

waves $1 \leq m \leq 3$ is studied. Vibration modes with a prevalent longitudinal u, circumferential v or radial w displacement component, which corresponds to a primarily axial, torsional or flexural vibration, respectively, are investigated.

From these comparisons, it can be observed that the percentage difference between the results of the two formulations is concentrated in the highest natural frequencies corresponding to the modal shape with prevalent radial displacement w, while elsewhere the percentage difference is negligible. The same result is found by comparing the natural frequencies of the present model in the isotropic form obtained via Ru's and He's formulations of the van der Waals interaction coefficient in Tables 3 and 4.

Starting from these results, in the following, only the highest radial natural frequencies will be considered to investigate the differences between the two formulations (Ru's vs He's) adopted for the simulation of the van der Waals interaction coefficient.

It should be underlined that, in a previous work of the same author, it was obtained that the differences in the results due to the different shell theory (Sanders vs. Donnell) considered to model the linear vibrations of DWCNTs are concentrated in the lowest radial natural frequencies, see Ref. [46] for more details.

Let us extend the previous analysis of Table 1 by considering the range of longitudinal half-waves $0 \leq m \leq 5$, the range of circumferential waves $0 \leq n \leq 8$ and the range of inner radius values 0.5 nm $\leq R_1 \leq$ 10 nm. In addition, on the basis of the previous results, let us focus our attention on the highest radial natural frequencies.

In Figures 4–8, the curves of the percentage differences between the natural frequencies of the simply supported DWCNT of Table 1 obtained by considering Ru's and He's formulations are shown, where the more accurate He's formulation is assumed as the reference. Vibration modes with a different number of waves along the longitudinal and circumferential directions (m, n) are analysed. Different values of inner radius R_1 are adopted. The aim of the present study is to investigate both applicability and limitations of Ru's formulation for vibration modelling of DWCNTs.

Table 5. Natural frequencies (THz) of the simply supported DWCNT of Table 1 with inner radius R_1 = 5 nm and aspect ratio L/R_2 = 10. Donnell shell theory. Anisotropic elastic shell model. Circumferential flexure modes (n = 2). Van der Waals interaction forces. Comparisons between Ru's (38) and He's (39) formulations.

		Natural Frequency (THz)			Diff. (%)
Mode (m,n)	**Prevalent Displacement**	**Prevalent Mode Shape**	**Anisotropic Model (Ru)**	**Anisotropic Model (He)**	
(1,2)	w	R_1	0.0162	0.0162	0.00
(2,2)	w	R_1	0.0510	0.0510	0.00
(3,2)	w	R_1	0.1023	0.1023	0.00
(1,2)	u	R_2	0.8593	0.8594	0.01
(2,2)	u	R_2	0.8936	0.8943	0.08
(1,2)	u	R_1	0.9160	0.9161	0.01
(3,2)	u	R_2	0.9421	0.9437	0.17
(2,2)	u	R_1	0.9538	0.9541	0.03
(3,2)	u	R_1	1.0149	1.0152	0.03
(1,2)	v	R_2	1.2975	1.3086	0.85
(2,2)	v	R_2	1.3462	1.3567	0.77
(3,2)	v	R_2	1.4230	1.4327	0.68
(1,2)	v	R_1	1.5248	1.5257	0.06
(2,2)	v	R_1	1.5550	1.5560	0.06
(3,2)	v	R_1	1.6063	1.6074	0.07
(1,2)	w	R_1	2.6313	2.8507	7.70
(2,2)	w	R_1	2.6319	2.8510	7.69
(3,2)	w	R_1	2.6329	2.8517	7.67

In Figure 4, a simply supported DWCNT with inner radius $R_1 = 0.5$ nm is considered. From this Figure, it is observed that the percentage difference assumes the initial value of 1.5% for $n = 0$. Then, it decreases to the local minimum of 0.4% for $n = 1$ and increases to the local maximum of 14% for $n = 2$. Finally, for $n \geq 3$ the percentage difference decreases very quickly with increasing n.

In Figure 5, a simply supported DWCNT with inner radius $R_1 = 1$ nm is analysed. From this Figure it is observed that the percentage difference assumes the initial value of 4% for $n = 0$. Then, it decreases to the local minimum of 1.5% for $n = 1$ and increases to the local maximum of 10.5% for $n = 2$. Finally, for $n \geq 3$ the percentage difference decreases quickly with increasing n.

In Figure 6, a simply supported DWCNT with inner radius $R_1 = 2$ nm is investigated. From this Figure, it is observed that the percentage difference assumes the initial value of 6% for $n = 0$. Then, it decreases to the local minimum of 1% for $n = 2$ and increases to the local maximum of 8% for $n = 4$. Finally, for $n \geq 5$ the percentage difference decreases very slowly with increasing n.

In Figure 7, a simply supported DWCNT with inner radius $R_1 = 5$ nm is examined. From this Figure, it is observed that the percentage difference assumes the initial value of 5.5% for $n = 0$, which is maintained quasi-constant for $n = (1,2)$. Then, it decreases to the local minimum of 2% for $n = 4$ and increases to the local maximum of 6% for $n = 6$, which is maintained quasi-constant with increasing n.

In Figure 8, a simply supported DWCNT with inner radius $R_1 = 10$ nm is studied. From this Figure, it is observed that the percentage difference assumes the initial value of 5% for $n = 0$, which is maintained quasi-constant for $1 \leq n \leq 4$. Then, it decreases slowly for $n = (5,6)$ and finally very quickly with increasing n.

From Figures 4–8 it is noted that, for all considered values of inner radius R_1, the behaviour is almost the same for every number of longitudinal half-waves m; therefore, the percentage differences of Figures 4–8 can be rightly synthesized in Figure 9, which shows the percentage differences between the highest radial natural frequencies obtained via Ru's (38) and He's (39) formulations for the inner radius range 0.5 nm $\leq R_1 \leq$ 10 nm and the number of longitudinal half-waves $m = 1$.

From Figure 9 it can be observed that, as the inner radius R_1 increases, the value of the initial percentage difference for $n = 0$ increases, converging to the final value of 5% for $R_1 = 10$ nm.

Again, as the inner radius R_1 increases, the oscillation amplitude of the portion of the percentage difference curve between the local minimum and maximum decreases, where the local minimum and maximum tend to approach, moving towards increasing numbers of circumferential waves n.

Finally, as the inner radius R_1 increases, the percentage difference curves tend to converge to the quasi-constant curve corresponding to $R_1 = 10$ nm, without maximum and minimum values and with the percentage difference close to 5%.

Since, in Section 5.2, it was derived that, for a sufficiently large inner radius, the interaction coefficient no longer depends on the radius, but it assumes a constant value, which is similar to Ru's and He's formulations, then, in the following, the limit value of applicability of Ru's formulation for the vibration modelling of DWCNTs will be imposed at 5%, which is the value of the quasi-constant percentage difference curve corresponding to $R_1 = 10$ nm.

From Figure 9, the following comments for increasing values of the inner radius R_1 can be made:

- for $n = (0,1)$ the percentage difference is initially very low ($< 2\%$), then it increases, finally stabilizing at 5%;
- for $n = 2$, the percentage difference is initially extremely high ($\approx 15\%$), then it decreases by assuming a minimum value of 2% and finally increases, stabilizing at 5%;

- for $n = 3$, the percentage difference is initially very high ($\approx 10\%$), then it reduces, stabilizing at 5%;
- for $n = 4$, the percentage difference is initially relatively low ($\approx 4\%$), then it increases until a maximum value of 10%, it decreases until a minimum value of 2% and finally it increases, stabilizing at 5%;
- for $5 \leq n \leq 8$, the percentage difference is initially very low ($< 2\%$), then it increases until a maximum value of 8% and finally decreases at a value lower than 5%.

Therefore, by assuming the more accurate He's formulation as a reference, considering the Donnell shell theory and adopting an anisotropic elastic shell model, from Figure 9, with respect to the number of circumferential waves n and as a function of the value of the inner radius R_1, the following ranges of applicability of Ru's formulation for vibration modelling of DWCNTs are identified (percentage difference $\leq 5\%$):

- $n = 0$ (axisymmetric modes), for every value of R_1;
- $n = 1$ (beam-like modes), for every value of R_1;
- $n = 2$ (circumferential flexure modes), for $R_1 \geq 2$ nm;
- $n = 3$ (shell-like modes), for $R_1 \geq 5$ nm;
- $n = (4,5)$ (shell-like modes), for $R_1 \leq 0.5$ nm and for $R_1 \geq 5$ nm;
- $n = 6$ (shell-like modes), for $R_1 \leq 0.5$ nm and for $R_1 \geq 10$ nm;
- $n = (7,8)$ (shell-like modes), for $R_1 \leq 1$ nm and for $R_1 \geq 10$ nm;

while the corresponding ranges of limitation of Ru's formulation for vibration modelling of DWCNTs are (percentage difference $> 5\%$):

- $n = 2$ (circumferential flexure modes), for $R_1 \leq 1$ nm;
- $n = 3$ (shell-like modes), for $R_1 \leq 2$ nm;
- $n = (4,5)$ (shell-like modes), for 1 nm $\leq R_1 \leq 2$ nm;
- $n = 6$ (shell-like modes), for 1 nm $\leq R_1 \leq 5$ nm;
- $n = (7,8)$ (shell-like modes), for 2 nm $\leq R_1 \leq 5$ nm.

Similarly, from Figure 9, with respect to the value of inner radius R_1 and as a function of the number of circumferential waves n, the following ranges of applicability of Ru's formulation for the vibration modelling of DWCNTs are identified (percentage difference $\leq 5\%$):

- $R_1 = 0.5$ nm (very low inner radius), for $n \leq 1$ and for $n \geq 4$;
- $R_1 = 1$ nm (low inner radius), for $n \leq 1$ and for $n \geq 7$;
- $R_1 = 2$ nm (intermediate inner radius), for $n \leq 2$;
- $R_1 = 5$ nm (high inner radius), for $n \leq 5$;
- $R_1 = 10$ nm (very high inner radius), for every number of n;

while the corresponding ranges of limitation of Ru's formulation for vibration modelling of DWCNTs are (percentage difference $> 5\%$):

- $R_1 = 0.5$ nm (very low inner radius), for $n = (2,3)$;
- $R_1 = 1$ nm (low inner radius), for $2 \leq n \leq 6$;
- $R_1 = 2$ nm (intermediate inner radius), for $n \geq 3$;
- $R_1 = 5$ nm (high inner radius), for $n \geq 6$.

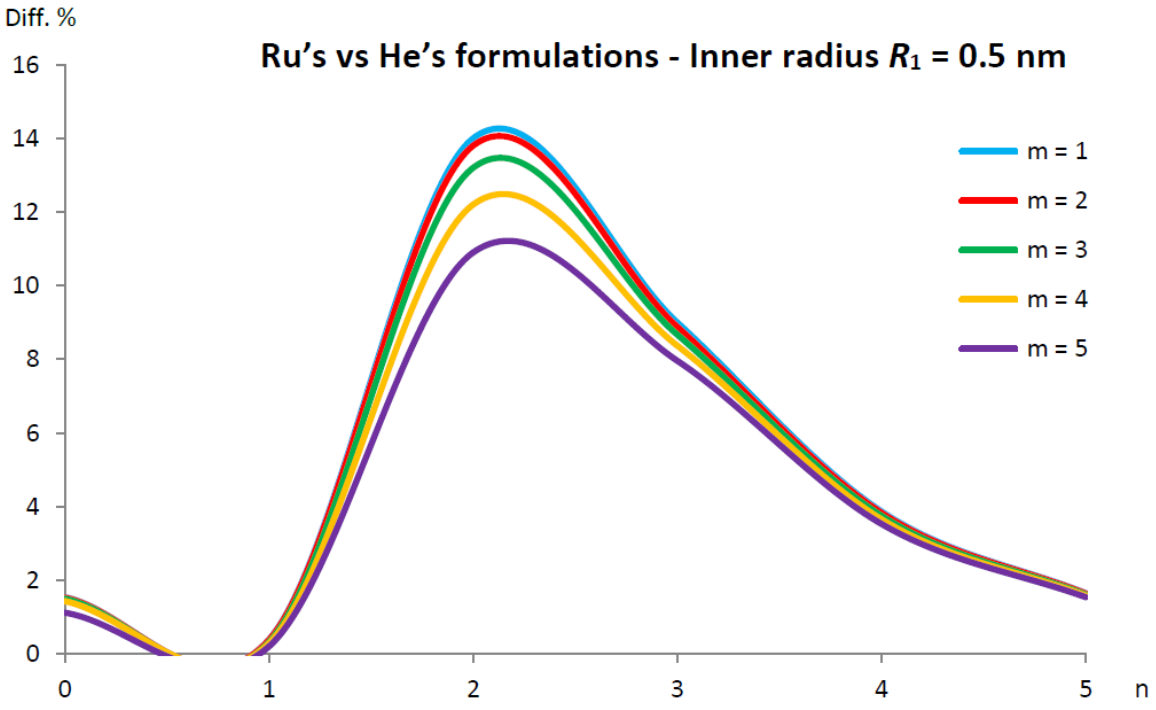

Figure 4. Percentage differences between the highest radial natural frequencies of the simply supported DWCNT of Table 1 with inner radius R_1 = 0.5 nm and aspect ratio L/R_2 = 10 from Ru's (38) and He's (39) formulations. Donnell shell theory. Anisotropic elastic shell model. Number of longitudinal half-waves *m*. Number of circumferential waves *n*.

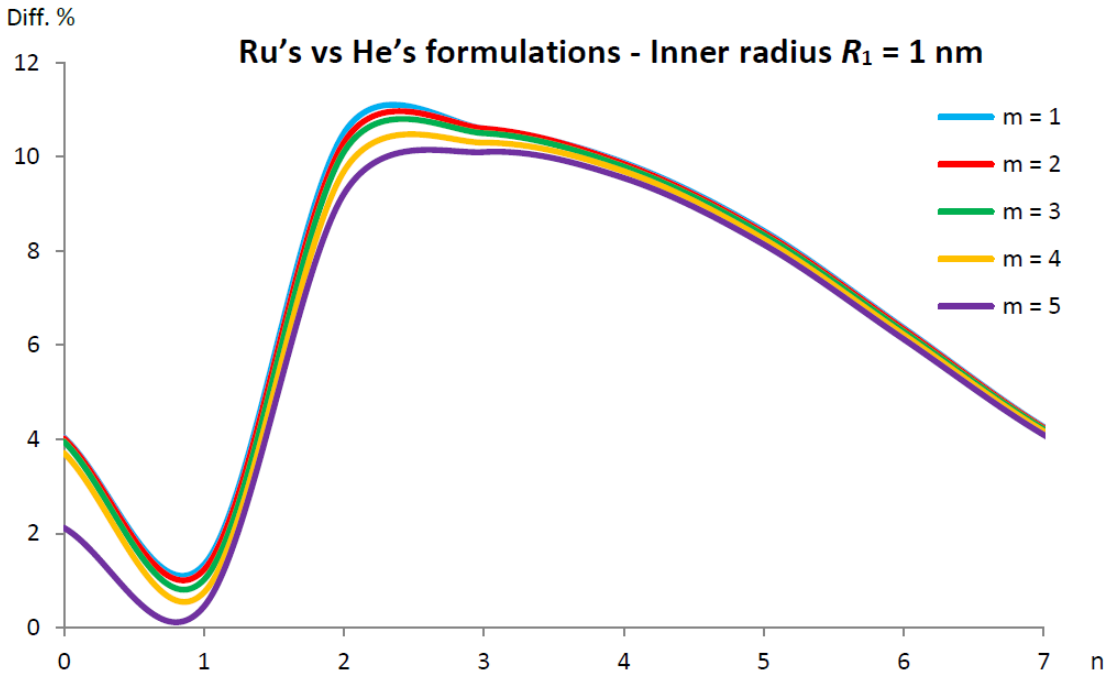

Figure 5. Percentage differences between the highest radial natural frequencies of the simply supported DWCNT of Table 1 with inner radius R_1 = 1 nm and aspect ratio L/R_2 = 10 from Ru's (38) and He's (39) formulations. Donnell shell theory. Anisotropic elastic shell model. Number of longitudinal half-waves *m*. Number of circumferential waves *n*.

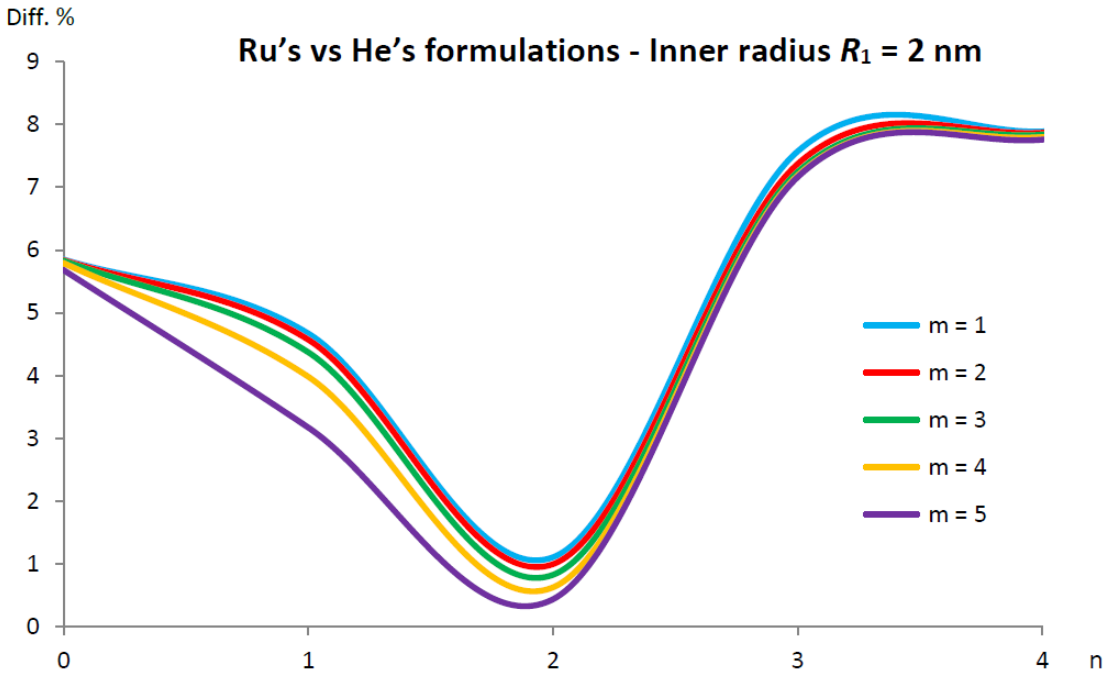

Figure 6. Percentage differences between the highest radial natural frequencies of the simply supported DWCNT of Table 1 with inner radius R_1 = 2 nm and aspect ratio L/R_2 = 10 from Ru's (38) and He's (39) formulations. Donnell shell theory. Anisotropic elastic shell model. Number of longitudinal half-waves *m*. Number of circumferential waves *n*.

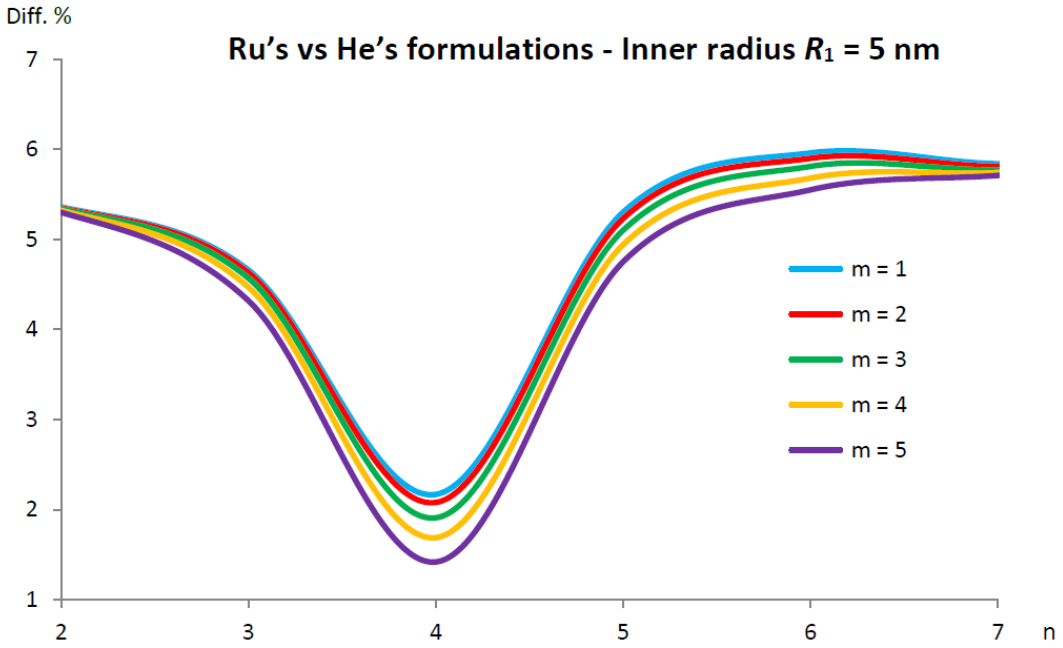

Figure 7. Percentage differences between the highest radial natural frequencies of the simply supported DWCNT of Table 1 with inner radius R_1 = 5 nm and aspect ratio L/R_2 = 10 from Ru's (38) and He's (39) formulations. Donnell shell theory. Anisotropic elastic shell model. Number of longitudinal half-waves *m*. Number of circumferential waves *n*.

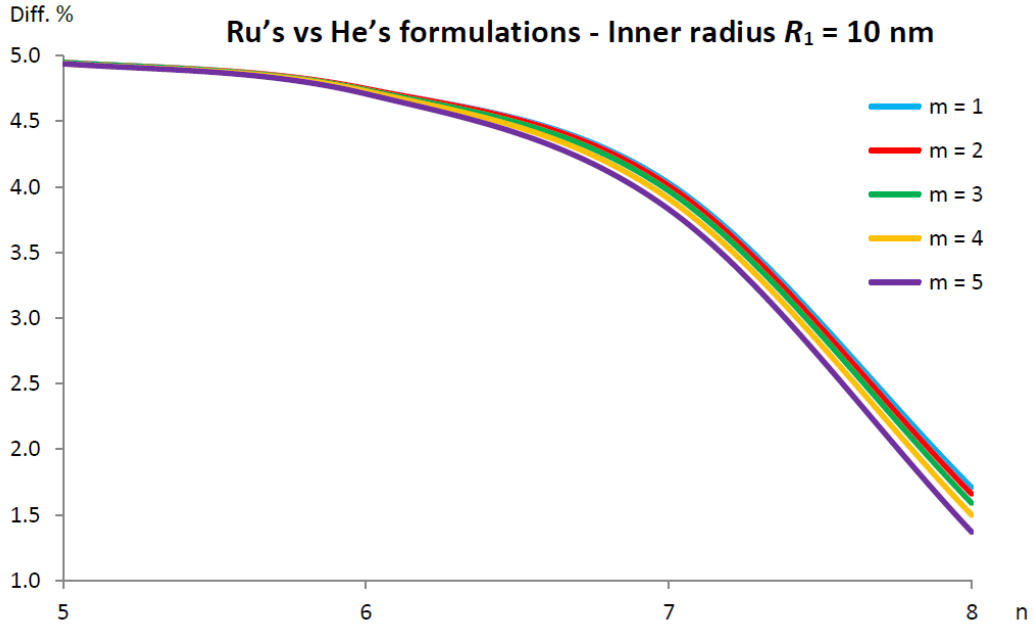

Figure 8. Percentage differences between the highest radial natural frequencies of the simply supported DWCNT of Table 1 with inner radius R_1 = 10 nm and aspect ratio L/R_2 = 10 from Ru's (38) and He's (39) formulations. Donnell shell theory. Anisotropic elastic shell model. Number of longitudinal half-waves m. Number of circumferential waves n.

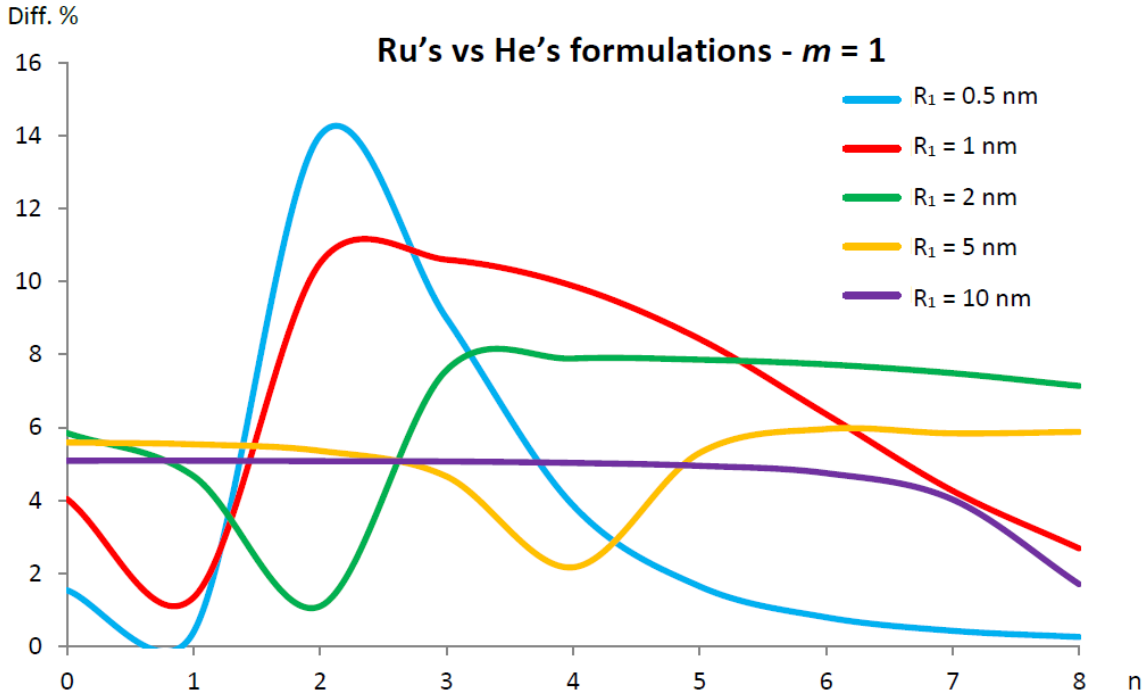

Figure 9. Percentage differences between the highest radial natural frequencies obtained via Ru's (38) and He's (39) formulations (He as reference). Donnell shell theory. Anisotropic elastic model. Simply supported DWCNT of Table 1 with m = 1 longitudinal half-wave and aspect ratio L/R_2 = 10. Inner radius R_1. Number of circumferential waves n.

As previously verified, the vibrational mode shapes, and the corresponding natural frequencies, of DWCNTs are sensitive to the van der Waals interactions. Actually, from Figure 3 it can be noted that the maximum difference between the values of Ru's and

He's van der Waals interaction coefficient is present at the inner radius R1 = 0.5 nm. So, the investigation of the critical order number (m, n) of the mode shape with which the difference between Ru's and He's formulations cannot be ignored should be carried out at that value of the inner radius, see Figure 4. First of all, from Figure 4 it can be observed that the behaviour is almost the same for every number of longitudinal half-waves m, and therefore, the analysis will be focused on the critical number of circumferential waves n. By imposing the limit value of percentage difference of 5%, below which Ru's formulation can be considered as sufficiently accurate, it is found that Ru's formulation cannot be applied in the range of the number of circumferential waves n = (2,3), which denotes the critical order number of the mode shapes.

In the end, we want to validate the previous assumption of Section 5.2, i.e., that it is necessary to assume an anisotropic model for $R_1 < 1$ nm (relatively small inner radius), while it can be adopted an isotropic model for $R_1 > 5$ nm (large inner radius).

In Figure 10, the percentage difference in curves between the highest radial natural frequencies obtained via He's formulation by adopting isotropic and anisotropic elastic shell models (anisotropic model as reference) are reported. He's formulation is applied since it takes into account the effect of the radius, and therefore, is able to simulate the actual anisotropic behaviour of CNTs more correctly than Ru's one. A simply supported DWCNT with an aspect ratio $L/R_2 = 10$ is analysed. The Donnell shell theory is adopted. Circumferential flexure modes ($n = 2$) are studied. Different values of inner radius R_1 and numbers of longitudinal half-waves m are investigated.

From this Figure, it is noted that, for a relatively small inner radius $R_1 < 1$ nm, the percentage difference is significant ($\approx 3.5\%$), and therefore, the anisotropic model must be adopted; conversely, for a large inner radius $R_1 > 5$ nm, the percentage difference is negligible ($< 0.2\%$), and therefore, within this range, the isotropic model can also be correctly adopted. Again, this behaviour is almost the same for every number of longitudinal half-waves m.

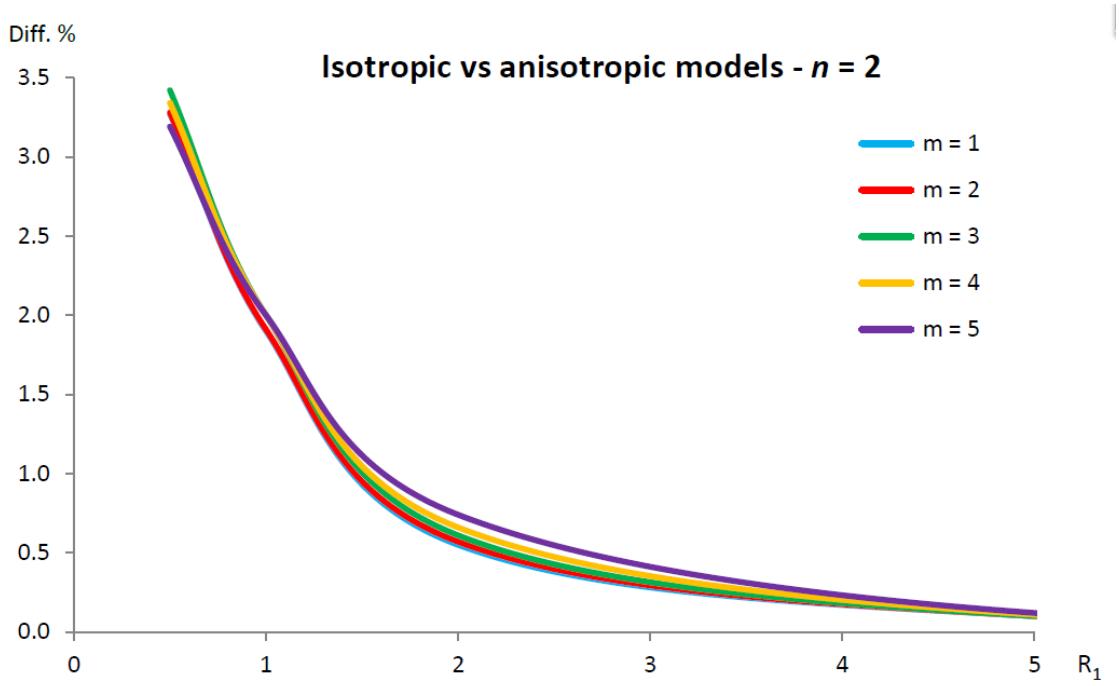

Figure 10. Percentage differences between the highest radial natural frequencies obtained via isotropic and anisotropic elastic shell models (anisotropic model as reference). Donnell shell theory. He's formulation (39). Simply supported DWCNT of Tables 1 and 2 with aspect ratio $L/R_2 = 10$ and $n = 2$. Inner radius R_1. Number of longitudinal half-waves m.

6. Conclusions

In the present paper, the comparison is conducted between Ru's and He's formulations of the van der Waals interaction coefficient for the evaluation of the natural frequencies of DWCNTs. The actual discrete DWCNT is modelled by means of a couple of concentric equivalent continuous cylindrical shells, where the Donnell shell theory is considered to obtain strain-displacement relationships and an anisotropic elastic shell model is adopted to take into account the chirality effects. Simply supported boundary conditions are imposed and Rayleigh–Ritz method is used to obtain approximate natural frequencies and mode shapes. Increasing values of the inner ratio R_1 are considered. Different numbers of longitudinal half-waves m and circumferential waves n are investigated.

The main findings are reported below:

1. for a small inner radius, the interaction coefficient strongly depends on the radius, and therefore it assumes very different values for Ru's and He's formulations;
2. for a large inner radius, the interaction coefficient no longer depends on the radius, and it assumes a constant value, which is similar for Ru's and He's formulations;
3. He's formulation is able to simulate the actual anisotropic behaviour of CNTs more accurately than Ru's formulation, and is assumed as reference for the comparisons;
4. the difference in the results between Ru's and He's formulations is localised in the highest radial natural frequencies;
5. for axisymmetric and beam-like modes, Ru's formulation can be applied for every value of the inner radius;
6. for shell-like modes with a relative low number of circumferential waves, Ru's formulation cannot be applied for a small inner radius;
7. for shell-like modes with a high number of circumferential waves, Ru's formulation can be applied for every value of the inner radius;
8. for a large inner radius, Ru's formulation can be applied for every number of circumferential waves;
9. the behaviour is almost the same for every number of longitudinal half-waves.

In all papers available in the literature that are focused on the analysis of MWCNT vibrations, the van der Waals interaction coefficient is always modelled by considering either Ru's or He's formulation. The main novelty of the present work is that, for the first time, the results of Ru's and He's formulations are compared with each other. From this comparison, which is carried out by varying DWCNT geometry and wavenumber, it is derived when it is possible to apply the less accurate but simpler Ru's formulation and when it is necessary to use the more accurate but also more complex He's formulation.

Funding: This research was funded by Department of Sciences and Methods for Engineering (University of Modena and Reggio Emilia) grant number 020142_22_FRN_SOSTEGNO_RICERCA_DISMI.

Acknowledgments: The Author is grateful to the Department of Sciences and Methods for Engineering of the University of Modena and Reggio Emilia (Grant 020142_22_FRN_SOSTEGNO_RICERCA_DISMI) for the financial support of the present work, which is dedicated to the blessed memory of Professor Leonid I. Manevitch, outstanding educator, respected teacher, admired scholar.

Conflicts of Interest: The authors declare no conflict of interest.

References

1. Iijima, S. Helical microtubules of graphitic carbon. *Nature* **1991**, *354*, 56–58. https://doi.org/10.1038/354056a0.
2. Ibrahim, K.S. Carbon nanotubes, properties and applications: A review. *Carbon Lett.* **2013**, *14*, 131–144.
3. Khan, D.; Ali, Z.; Asif, D.; Panjwani, M.K.; Khan, I. Incorporation of carbon nanotubes in photoactive layer of organic solar cells. *Ain Shams Eng. J.* **2021**, *12*, 897–900. https://doi.org/10.1016/j.asej.2020.06.002.
4. Luo, C.; Xie, H.; Wang, Q.; Luo, G.; Liu, C. A Review of the Application and Performance of Carbon Nanotubes in Fuel Cells. *J. Nanomater.* **2015**, *2015*, 4. https://doi.org/10.1155/2015/560392.
5. Rao, A.M.; Richter, E.; Bandow, S.; Chase, B.; Eklund, P.C.; Williams, K.A.; Fang, S.; Subbaswamy, K.R.; Menon, M.; Thess, A.; et al. Diameter-Selective Raman Scattering from Vibrational Modes in Carbon Nanotubes. *Science* **1997**, *275*, 187–191. https://doi.org/10.1126/science.275.5297.187.
6. Bandow, S.; Asaka, S.; Saito, Y.; Rao, A.M.; Grigorian, L.; Richter, E.; Eklund, P.C. Effect of the Growth Temperature on the Diameter Distribution and Chirality of Single-Wall Carbon Nanotubes. *Phys. Rev. Lett.* **1998**, *80*, 3779–3782. https://doi.org/10.1103/physrevlett.80.3779.
7. Dresselhaus, G.; Dresselhaus, M.S.; Hafner, J.H.; Hunter, M.; Jorio, A.; Lieber, C.M.; McClure, T.; Saito, R. Structural (n, m) Determination of Isolated Single-Wall Carbon Nanotubes by Resonant Raman Scattering. *Phys. Rev. Lett.* **2001**, *86*, 1118. https://doi.org/10.17877/de290r-6258.
8. Gupta, S.S.; Bosco, F.G.; Batra, R.C. Breakdown of structural models for vibrations of single-wall zigzag carbon nanotubes. *J. Appl. Phys.* **2009**, *106*, 063527. https://doi.org/10.1063/1.3232206.
9. Cheng, H.C.; Liu, Y.L.; Wu, C.; Chen, W.H. On radial breathing vibration of carbon nanotubes. *Comput. Methods Appl. Mech. Eng.* **2010**, *199*, 2820–2827.
10. Duan, W.H.; Wang, C.; Zhang, Y. Calibration of nonlocal scaling effect parameter for free vibration of carbon nanotubes by molecular dynamics. *J. Appl. Phys.* **2007**, *101*, 024305. https://doi.org/10.1063/1.2423140.
11. Odegard, G.M.; Gates, T.S.; Nicholson, L.M.; Wise, K.E. Equivalent-Continuum Modeling of Nano-Structured Materials. *Compos. Sci. Technol.* **2002**, *62*, 1869–1880.
12. Arroyo, M.; Belytschko, T. Continuum Mechanics Modeling and Simulation of Carbon Nanotubes. *Meccanica* **2005**, *40*, 455–469. https://doi.org/10.1007/s11012-005-2133-y.
13. Zhang, P.; Huang, Y.; Geubelle, P.H.; Hwang, K. On the continuum modeling of carbon nanotubes. *Acta Mech. Sin.* **2002**, *18*, 528–536. https://doi.org/10.1007/bf02486577.
14. Yakobson, B.I.; Brabec, C.J.; Bernholc, J. Nanomechanics of Carbon Tubes: Instabilities beyond Linear Response. *Phys. Rev. Lett.* **1996**, *76*, 2511–2514. https://doi.org/10.1103/physrevlett.76.2511.
15. Wang, C.; Ru, C.Q.; Mioduchowski, A. Applicability and Limitations of Simplified Elastic Shell Equations for Carbon Nanotubes. *J. Appl. Mech.* **2004**, *71*, 622–631. https://doi.org/10.1115/1.1778415.
16. Silvestre, N.; Wang, C.; Zhang, Y.; Xiang, Y. Sanders shell model for buckling of single-walled carbon nanotubes with small aspect ratio. *Compos. Struct.* **2011**, *93*, 1683–1691. https://doi.org/10.1016/j.compstruct.2011.01.004.
17. Silvestre, N. On the accuracy of shell models for torsional buckling of carbon nanotubes. *Eur. J. Mech.-A/Solids* **2012**, *32*, 103–108. https://doi.org/10.1016/j.euromechsol.2011.09.005.
18. Strozzi, M.; Manevitch, L.I.; Pellicano, F.; Smirnov, V.V.; Shepelev, D.S. Low-frequency linear vibrations of single-walled carbon nanotubes: Analytical and numerical models. *J. Sound Vib.* **2014**, *333*, 2936–2957. https://doi.org/10.1016/j.jsv.2014.01.016.
19. Strozzi, M.; Smirnov, V.V.; Manevitch, L.I.; Pellicano, F. Nonlinear vibrations and energy exchange of single-walled carbon nanotubes. Radial breathing modes. *Compos. Struct.* **2018**, *184*, 613–632. https://doi.org/10.1016/j.compstruct.2017.09.108.
20. Strozzi, M.; Pellicano, F. Nonlinear Resonance Interaction between Conjugate Circumferential Flexural Modes in Single-Walled Carbon Nanotubes. *Shock Vib.* **2019**, *2019*, 3241698. https://doi.org/10.1155/2019/3241698.
21. Strozzi, M.; Smirnov, V.V.; Manevitch, L.I.; Pellicano, F. Nonlinear normal modes, resonances and energy exchange in single-walled carbon nanotubes. *Int. J. Non-Linear Mech.* **2020**, *120*, 103398.
22. Chang, T.; Geng, J.; Guo, X. Prediction of chirality- and size-dependent elastic properties of single-walled carbon nanotubes via a molecular mechanics model. *Proc. R. Soc. A Math. Phys. Eng. Sci.* **2006**, *462*, 2523–2540. https://doi.org/10.1098/rspa.2006.1682.
23. Chang, T. A molecular based anisotropic shell model for single-walled carbon nanotubes. *J. Mech. Phys. Solids* **2010**, *58*, 1422–1433. https://doi.org/10.1016/j.jmps.2010.05.004.
24. Ghavanloo, E.; Fazelzadeh, S. Vibration characteristics of single-walled carbon nanotubes based on an anisotropic elastic shell model including chirality effect. *Appl. Math. Model.* **2012**, *36*, 4988–5000. https://doi.org/10.1016/j.apm.2011.12.036.
25. Fazelzadeh, S.A.; Ghavanloo, E. Nonlocal anisotropic elastic shell model for vibrations of single-walled carbon nanotubes with arbitrary chirality. *Compos. Struct.* **2012**, *94*, 1016–1022. https://doi.org/10.1016/j.compstruct.2011.10.014.
26. Leissa, A.W. *Vibration of Shells*; Acoustical Society of America: Columbus, Ohio, 1993.
27. Yamaki, N.; Simitses, G.J. Elastic Stability of Circular Cylindrical Shells. *J. Appl. Mech.* **1985**, *52*, 501–502. https://doi.org/10.1115/1.3169089.
28. Soedel, W.; Qatu, M.S. Vibrations of Shells and Plates, Third Edition. *J. Acoust. Soc. Am.* **2005**, *117*, 1683. https://doi.org/10.1121/1.1873932.
29. Ventsel, E.; Krauthammer, T.; Carrera, E. Thin Plates and Shells: Theory, Analysis, and Applications. *Appl. Mech. Rev.* **2002**, *55*, B72–B73. https://doi.org/10.1115/1.1483356.

30. Jones, J.E. On the determination of molecular fields.—I. From the variation of the viscosity of a gas with temperature. *Proc. R. Soc. London. Ser. A Math. Phys. Sci.* **1924**, *106*, 441–462. https://doi.org/10.1098/rspa.1924.0081.
31. Ru, C.Q. Elastic Models for Carbon Nanotubes. *Encycl. Nanosci. Nanotechnol.* **2004**, *2*, 731–744.
32. Ru, C.Q. Axially compressed buckling of a double-walled carbon nanotube embedded in an elastic medium. *J. Mech. Phys. Solids* **2001**, *49*, 1265–1279.
33. Ru, C.Q. Column buckling of multiwalled carbon nanotubes with interlayer radial displacements. *Phys. Rev. B* **2000**, *62*, 16962–16967. https://doi.org/10.1103/physrevb.62.16962.
34. Girifalco, L.A.; Lad, R.A. Energy of Cohesion, Compressibility, and the Potential Energy Functions of the Graphite System. *J. Chem. Phys.* **1956**, *25*, 693–697. https://doi.org/10.1063/1.1743030.
35. Pentaras, D.; Elishakoff, I. Effective Approximations for Natural Frequencies of Double-Walled Carbon Nanotubes Based on Donnell Shell Theory. *J. Nanotechnol. Eng. Med.* **2011**, *2*, 021013. https://doi.org/10.1115/1.4003601.
36. Elishakoff, I.; Pentaras, D. Fundamental natural frequencies of double-walled carbon nanotubes. *J. Sound Vib.* **2009**, *322*, 652–664. https://doi.org/10.1016/j.jsv.2009.02.037.
37. Pentaras, D.; Elishakoff, I. Free vibration of triple-walled carbon nanotubes. *Acta Mech.* **2011**, *221*, 239–249. https://doi.org/10.1007/s00707-011-0496-9.
38. Ehteshami, H.; Hajabasi, M.A. Analytical approaches for vibration analysis of multi-walled carbon nanotubes modeled as multiple nonlocal Euler beams. *Phys. E Low-Dimens. Syst. Nanostructures* **2011**, *44*, 270–285. https://doi.org/10.1016/j.physe.2011.08.023.
39. Xu, K.Y.; Guo, X.N.; Ru, C.Q. Vibration of a double-walled carbon nanotube aroused by nonlinear intertube van der Waals forces. *J. Appl. Phys.* **2006**, *99*, 064303. https://doi.org/10.1063/1.2179970.
40. Xu, K.-Y.; Aifantis, E.C.; Yan, Y.-H. Vibrations of Double-Walled Carbon Nanotubes With Different Boundary Conditions Between Inner and Outer Tubes. *J. Appl. Mech.* **2008**, *75*, 021013. https://doi.org/10.1115/1.2793133.
41. He, X.; Kitipornchai, S.; Liew, K. Buckling analysis of multi-walled carbon nanotubes: A continuum model accounting for van der Waals interaction. *J. Mech. Phys. Solids* **2005**, *53*, 303–326. https://doi.org/10.1016/j.jmps.2004.08.003.
42. He, X.Q.; Eisenberger, M.; Liew, K.M. The effect of van der Waals interaction modeling on the vibration characteristics of multiwalled carbon nanotubes. *J. Appl. Phys.* **2006**, *100*, 124317. https://doi.org/10.1063/1.2399331.
43. He, X.Q.; Kitipornchai, S.; Wang, C.; Liew, K. Modeling of van der Waals force for infinitesimal deformation of multi-walled carbon nanotubes treated as cylindrical shells. *Int. J. Solids Struct.* **2005**, *42*, 6032–6047. https://doi.org/10.1016/j.ijsolstr.2005.03.045.
44. Strozzi, M.; Pellicano, F. Linear vibrations of triple-walled carbon nanotubes. *Math. Mech. Solids* **2018**, *23*, 1456–1481.
45. Strozzi, M.; Gendelman, O.; Elishakoff, I.; Pellicano, F. Applicability and Limitations of Simplified Elastic Shell Theories for Vibration Modelling of Double-Walled Carbon Nanotubes. *C* **2021**, *7*, 61. https://doi.org/10.3390/c7030061.
46. Strozzi, M.; Elishakoff, I.E.; Manevitch, L.I.; Gendelman, O.V. Applicability and limitations of Donnell shell theory for vibration modelling of double-walled carbon nanotubes. *Thin-Walled Struct.* **2022**, *178*, 109532. https://doi.org/10.1016/j.tws.2022.109532.
47. Strozzi, M.; Smirnov, V.V.; Pellicano, F.; Kovaleva, M. Nonlocal anisotropic elastic shell model for vibrations of double-walled carbon nanotubes under nonlinear van der Waals interaction forces. *Int. J. Non-Linear Mech.* **2022**, *146*, 104172. https://doi.org/10.1016/j.ijnonlinmec.2022.104172.
48. Natsuki, T.; Ni, Q.-Q.; Endo, M. Analysis of the vibration characteristics of double-walled carbon nanotubes. *Carbon* **2008**, *46*, 1570–1573. https://doi.org/10.1016/j.carbon.2008.06.058.
49. Natsuki, T.; Lei, X.-W.; Ni, Q.-Q.; Endo, M. Free vibration characteristics of double-walled carbon nanotubes embedded in an elastic medium. *Phys. Lett. A* **2010**, *374*, 2670–2674. https://doi.org/10.1016/j.physleta.2010.04.040.
50. Kumar, B.R. Investigation on mechanical vibration of double-walled carbon nanotubes with inter-tube van der Waals forces. *Adv. Nano Res.* **2018**, *6*, 135–145.
51. Afsharirad, F.; Mousanezhad, S.; Biglari, H.; Rahmani, O. Molecular dynamics of axial interwall van der Waals force and mechanical vibration of double-walled carbon nanotubes. *Mater. Today Commun.* **2021**, *28*, 102708. https://doi.org/10.1016/j.mtcomm.2021.102708.
52. Asghar, S.; Naeem, M.N.; Hussain, M. Non-local effect on the vibration analysis of double walled carbon nanotubes based on Donnell shell theory. *Phys. E Low-Dimens. Syst. Nanostructures* **2020**, *116*, 113726. https://doi.org/10.1016/j.physe.2019.113726.
53. Gul, U.; Aydogdu, M. Noncoaxial vibration and buckling analysis of embedded double-walled carbon nanotubes by using doublet mechanics. *Compos. Part B: Eng.* **2018**, *137*, 60–73. https://doi.org/10.1016/j.compositesb.2017.11.005.
54. Senthilkumar, V. Axial vibration of double-walled carbon nanotubes using double-nanorod model with van der Waals force under Pasternak medium and magnetic effects. *Vietnam J. Mech.* **2022**, *44*, 29–43. https://doi.org/10.15625/0866-7136/16582.
55. Natsuki, J.; Wu, P.; Jiang, H.; Natsuki, T. Dynamic analysis of double-walled carbon nanotubes embedded in elastic medium under a nanoparticle delivery. *Diam. Relat. Mater.* **2022**, *128*, 109194. https://doi.org/10.1016/j.diamond.2022.109194.